Archives of Toxicology
https://doi.org/10.1007/s00204-025-04103-2

REGULATORY TOXICOLOGY

Deriving safe limits for N-nitroso-bisoprolol by error-corrected next-generation sequencing (ecNGS) and benchmark dose (BMD) analysis, integrated with QM modeling and CYP-docking analysis

Stephanie Simon[1] · Jörg Schlingemann[1] · George Johnson[2] · Christian Brenneis[1] · Brunhilde Guessregen[3] · Jakub Kostal[4,5] · Jessica Dieckhoff[1]

Received: 2 May 2025 / Accepted: 26 May 2025

Abstract

N-nitroso-bisoprolol (NBP) is a nitrosamine drug substance-related impurity (NDSRI) of bisoprolol, which is used to treat cardiac diseases since decades. To investigate the mutagenic potential of NBP, in vitro methods such as Enhanced Ames Test (EAT) and a mammalian cell gene mutation (HPRT) assay were used. To assess the in vivo mutagenicity, a 28-day repeat-dose study was conducted in wild-type NMRI mice, and liver and bone marrow samples were subjected to error-corrected next-generation sequencing (i.e., duplex sequencing) followed by benchmark dose analysis (BMD). NBP did not show mutagenic effects in Ames tests using 10 % and 30 % induced rat or 30 % uninduced hamster S9. However, relevant increases in mutation frequencies were observed in an EAT in the presence of 30 % induced hamster S9 in strains TA100 and TA1535, confirming that the most stringent conditions of the EAT are appropriate to detect the mutagenic activity of weak mutagens, such as NBP. In the HPRT assay conducted in V79 cells, nitroso-diethylamine (NDEA) relevantly induced the mutation frequency, but not NBP. The highly sensitive error-corrected Next-Generation Sequencing (ecNGS) method to detect mutations across the genome represents an appropriate in vivo mutagenicity investigation equally suitable as a TGR assay to assess the mutagenic potential of nitrosamines. A weak induction of mutation frequencies was detected by ecNGS in the liver and the bone marrow of mice. Using BMD analysis, new safe limits were calculated for NBP, which are higher than the published AI of 1.5 µg/person/day. Using the approach to calculate Permissible Daily Exposure (PDE) limits according to ICH Q3C, a lifetime PDE of 400 µg/person/day was derived. Based on the ICH M7 framework for derivation of Acceptable Intake (AI) limits, an AI of 64 µg/person/day was established. Consistent with regulatory emphasis on mechanistic interpretation, in vivo modeling was further supported by in silico calculations. Specifically, the validated Computer-Aided Discovery and RE-design (CADRE) tool was used to predict the potency of NBP and further differentiate its metabolic activity from the anchor nitrosamine NDEA via quantum mechanics (QM) calculations and CYP-binding predictions. Outcomes of this analysis were consistent with in vivo studies, while offering a deeper understanding of the fundamental biochemistry using a physics-led method. The integrated in vivo–in silico investigation provides a data-based determination of safe limits, suggesting that the AI based on structural considerations solely might be over-conservative and should not be capped at the TTC.

✉ Jörg Schlingemann
joerg.schlingemann@merckgroup.com

1 Merck Healthcare KGaA, Darmstadt, Germany

2 Swansea University Medical School, Swansea SA8PP, UK

3 Merck KGaA, Darmstadt, Germany

4 DOT Consulting LLC, Alexandria, VA 22314, USA

5 The George Washington University, 800 22nd ST NW, Washington DC 20052, USA

Published online: 11 June 2025

Highlights

- First presentation of in vivo mutagenicity data for an NDSRI of a beta-blocker
- Nitroso-bisoprolol was not mutagenic in standard and modified Ames tests using rat or uninduced hamster S9, but positive in EAT with 30 % induced hamster S9
- ecNGS revealed a low mutagenic potential, suggesting that nitroso-bisoprolol is not in the cohort-of-concern
- Using benchmark dose analysis, new safe limits far above the published 1.5 µg/day could be derived, suggesting that the CPCA based on SAR considerations solely is over-sensitive and should not be capped at the TTC.
- The new safe limits for one beta-blocker determined in the present work may serve as blueprint for class-specific PDE or AI to be applied to NDSRIs that bear an isopropyl or tert-butyl group connected to the nitroso group.
- Horizontally integrated in silico–in vivo analysis shows good agreement between CADRE (QM) outcomes, augmented here with CYP-docking analysis, and in vivo results
- In silico (QM) models can be used a priori to gauge feasibility of a higher AI and/or post in vivo studies to gain greater confidence in the proposed limit based on mechanistic interpretation

Keywords Nitroso-bisoprolol · Beta-blocker · Nitrosamines · NDSRI · Mutagenicity · ecNGS · Duplex sequencing · Benchmark dose analysis (BMD) · Acceptable intake · AI · Permissible (permitted) daily exposure · PDE · In-silico modeling · Quantum mechanics · CYP docking · Predictive toxicology

Introduction

N-nitrosamines belong to a class of N-nitroso compounds, which are referred to as members of the cohort-of-concern carcinogens according to the ICH M7 guideline, as some of them of are known potent rodent carcinogens and thus potential human carcinogens (ICH 2023). N-nitrosamine contaminations have been a point of concern for pharmaceutical manufacturers and regulators alike since their first discovery in batches of the angiotensin II receptor antagonist valsartan in late 2018 (Nudelman et al. 2023). While first reports concerned the small and potent dialkyl nitrosamines, such as nitroso-dimethylamine (NDMA) and nitroso-dieethylamine (NDEA), it was soon discovered that there is a second dimension related to N-nitrosamines derived from vulnerable Active Pharmaceutical Ingredients (APIs) and impurities, especially those that are secondary amines. Due to their structural similarity to the drug or fragments of the drug, those N-nitrosamines are referred to as "nitrosamine drug substance-related impurities" (NDSRIs) (EMA 2024a; FDA 2024). It was shown that this concerns a considerable percentage of available medicines, putting whole classes of drugs at risk of forming N-nitrosamines (Schlingemann et al. 2023). One of these classes are agents targeting the adrenergic beta receptors, which comprises both respective agonists and antagonists, the latter also being known as beta-blockers. An overview on common beta agonists and antagonists is provided as supplementary information.

Bisoprolol is a beta1-selective-adrenoceptor blocking agent (β-blocker) used in the treatment of cardiovascular diseases, such as hypertension, angina pectoris, and heart failure. It is included in the WHO list of essential medicines (WHO 2023). All β-blockers and β-agonists share a common structural motif that includes a hydroxyl group and a secondary amine functionality. For this reason, the whole class of compounds is at risk of forming N-nitrosamines under promoting conditions, i.e., in the presence of nitrosating agents. Nitroso-bisoprolol (NBP) is an NDSRI of bisoprolol. The chemical structures of bisoprolol and NBP are shown in Fig. 1.

Regulatory agencies, such as EMA and U.S. FDA, have set provisional acceptable daily intake levels for a growing number of nitrosamines either calculated from TD_{50} values of lifetime rodent carcinogenicity studies, determined by extrapolation from close analogues (read-across), derived by the Carcinogenicity Potency Categorization Approach (CPCA) or based on Enhanced Ames Test (EAT) and/or in vivo mutagenicity data (EMA 2024b; FDA 2023; Kruhlak et al. 2024). The acceptable intake (AI) for NBP and most other NDSRIs from this class of medicines has been set to 1500 ng/day (EMA 2024b). While carcinogenicity data are available for many of the low-molecular-weight nitrosamines such as NDMA or NDEA, these data are and will not be available for most of the NDSRIs. This lack of data leads to uncertainties how to derive realistic and safe AI levels for NDSRIs across industry and regulatory agencies. The CPCA first introduced by Health Authorities (HA) in 2023 was a

major step forward in the assessment and control of nitrosamines as it allowed a rapid and consistent assignment of provisional AIs to a large number of NDSRIs in the absence of any compound-specific data and reduced some uncertainties significantly (Bercu et al. 2024; EMA 2023; FDA 2024; Ponting et al. 2024). However, the perception of the CPCA differs between HAs. While it is generally accepted that the CPCA is a conservative approach, EMA considers all four options for nitrosamines without substance-specific data as described above equally suitable, whereas FDA seems to prefer the CPCA AI as the default (Kruhlak et al. 2024).

The bacterial reverse mutation (Ames) test is commonly accepted to assess the mutagenic potential of chemicals, including impurities (ICH 2023). To address concerns from HAs that the Ames standard protocols according to OECD 471 (OECD 2020) might not be sensitive enough to detect the mutagenicity of nitrosamines, considerable work has been conducted by industry and within agencies. As a first result, the Enhanced Ames Test (EAT) protocol was published by EMA in 2023, other health authorities followed that approach (Canada 2024; EMA 2024c; FDA 2023). The recommended conditions include the use of the pre-incubation method (30 min pre-incubation time), the application of 30 % induced rat as well as 30 % induced hamster S9, the inclusion of two additional nitrosamine controls, e.g., NDMA or CPNP and the use of the lowest volume of organic solvent as possible (EMA 2024c). A large ring trial was initiated by the Health and Environmental Science Institute (HESI) Genetic Toxicology Technical Committee (GTTC) nitrosamine subgroup involving more than 20 companies, institutions, and agencies to investigate the "Concordance between Ames and Rodent Carcinogenicity Outcomes for *N*-Nitrosamines (NAs) with Rat and Hamster Metabolic Conditions" and to identify the most sensitive Ames conditions. The results of this ring trial were presented on a joint FDA-CDER/HESI meeting and recently published by the working group (Bercu et al. 2025). In this ring trial, 30 % induced hamster S9 showed the highest sensitivity. It was agreed that both *E. coli* WP2*uvrA* strains (with or without plasmid) were equally suitable. Also, DMSO was considered an appropriate solvent (Bercu et al. 2025). There is still debate on whether nitrosamine positive controls should be included and if, which ones to use. To investigate suitable solvents and volumes further, an initiative has been started by the Lhasa Complex Nitrosamine Consortium in collaboration with industry members. In the light of the acceptability of negative EAT results, there are also differing requirements by HAs. EMA and other agencies allow control of a nitrosamine tested negative in an EAT at 1.5 µg/day (Canada 2024; EMA 2024a). The FDA guidance remains less specific on this point and the agency may request additional data to support a 1.5 µg/day limit (FDA 2023). Until now, it is not specified which data might be requested, however, e.g., in vitro mammalian cell mutagenicity or in vitro metabolism data have been discussed. These discrepancies between HAs are still challenging for industry as there is uncertainty on which data may be ultimately requested.

To achieve limits above 1.5 µg/day, EMA recommends using either a read-across approach from a suitable surrogate molecule with carcinogenicity data or data from a "relevant, well conducted in vivo mutagenicity study" and allows control of a nitrosamine to ICH Q3A/B levels, if the result is negative (EMA 2024a). As the type of study is not specified further, there is ongoing debate on which of the available in vivo mutagenicity assays is acceptable for HAs. For many years, in vivo mutagenicity assays using transgenic rodents such as Big Blue® or MutaMouse® were the assays of choice and are widely accepted by authorities. However, in the light of the nitrosamine topic, sequencing methods such as error-corrected Next-Generation Sequencing [i.e., Duplex Sequencing (DS)] evolved considerably and gained more and more importance as an in vivo mutagenicity method to detect even rare mutations (Marchetti et al. 2023a, 2023b; Salk and Kennedy 2020; Valentine et al. 2020). The properties of TGR and DS are summarized in Table 1.

Error-corrected next-generation sequencing (ecNGS) allows for the detection of locus mutations across the entire genome, enabling a broader and more detailed assessment of mutational events in higher resolution, without the requirement of genetically modified animals. Duplex sequencing (DS) is a double-stranded tag-based error correction technology commercialized by TwinStrand Biosciences that

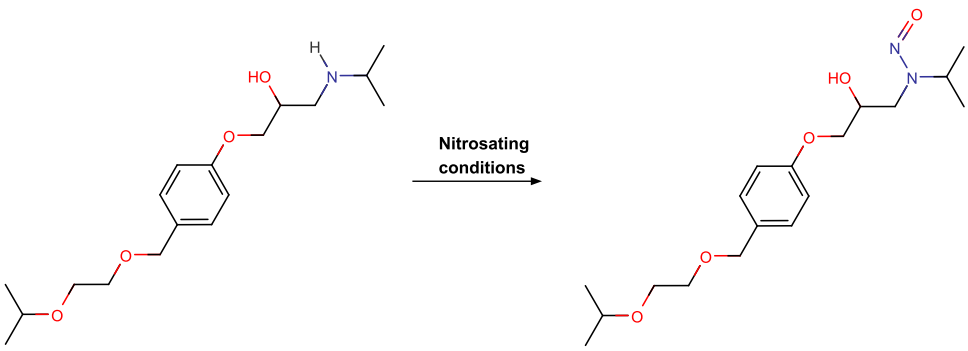

Fig. 1 Chemical structures of Bisoprolol (left) and Nitroso-bisoprolol (NBP) (right)

highly improves the accuracy of NGS providing a suitable method to identify also rare mutations in all kinds of tissues or cells and across all species (Salk and Kennedy 2020; Smith-Roe et al. 2023a; Valentine et al. 2020). DS achieves a sensitivity and specificity several orders of magnitude greater than other sequencing methods that do not consider paired-stranded information. Moreover, it is uniquely able to resolve mutants at the real-world frequencies produced by mutagens, i.e., on the order of 1 in 10 million (Salk and Kennedy 2020). The major advantage of ecNGS/DS over existing mutagenicity assays is its ability to directly detect chemically induced mutations in a genome-representative manner with high fidelity at the native DNA level. The data allow for highly quantitative assessments of mutation frequency (MF), mutation spectra, and trinucleotide mutation signatures (LeBlanc et al. 2022; Smith-Roe et al. 2023a).

In the field of genetic toxicology, the quantitative analysis of in vivo mutagenicity data becomes more and more important. Many researchers have proposed the use of dose–response data from in vivo genetic toxicity studies to determine Point of Departure (PoD) metrics such as the benchmark dose lower confidence interval (BMDL), to be used to establish human exposure limits for regulatory decision-making, namely tolerable daily intake or permissible daily exposure (Johnson et al. 2021; Wills et al. 2016a, b; Zeller et al. 2018).

The benchmark dose approach (BMD) provides an estimate of the dose that will elicit a small, pre-specified effect-size called the benchmark response (BMR). The response change value employed for BMD determination, which is often expressed as a fractional change relative to control (e.g., 50 % increase), is referred to as the Critical Effect Size (CES) or Benchmark Response (BMR). A CES of 50 % has been shown for other in vivo genetic toxicity endpoints and there is ongoing work to assess this for ecNGS; however, current best practice is to use a CES of 50 % for ecNGS in vivo as well (Bercu et al. 2016, 2023; Zeller et al. 2017; Zhang et al. 2024).

Recent publications comparing the sensitivity of different methods showed that DS is at least as sensitive as the transgenic mutagenicity readout (Bercu et al. 2023; Smith-Roe et al. 2023b; Zhang et al. 2024). Zhang et al. investigated the genotoxicity of N-nitroso-diethylamine (NDEA) using three in vivo mutagenicity assays: Comet, TRG (BigBlue®) and DS. DS was the most sensitive test in this comparison followed by BigBlue® and Comet, whereby the DS and TGR led to almost identical BMDLs. BMD modeling was applied to determine thresholds for genotoxic effects. These thresholds are valuable to calculate compound-specific AI limits, emphasizing a precautionary approach to managing exposure (Bercu et al. 2023; Zhang et al. 2024).

The ICH framework (ICH 2023, 2024) states that for mutagenic impurities, when a 'threshold mechanism' can be defined, a permitted daily exposure (PDE) calculation can be used. This was discussed within a Health and Environmental Sciences Institute (HESI) Genetic Toxicology Technical Committee (GTTC) publication (Johnson et al. 2021). Nitrosamines are generally within the cohort of concern (CoC) (ICH 2023), and due to the potency of some substances within this chemical class, regulatory bodies are currently reluctant to accept the threshold mechanism and PDE for any nitrosamine. However, analysis of mutation spectra of NBP compared to those of other nitrosamines also suggests a threshold mechanism for the DNA repair of NBP-induced mutations via methylguanine-methyltransferase (MGMT) (Fahrer and Christmann 2023). At the current time, there are building data to support relative potency of in vivo mutation compared to AI calculated using in vivo cancer bioassay data for nitrosamines (Johnson 2024; Jolly et al. 2024, 2025; Powley et al. 2024). A relative potency approach enables the calculation of AI using in vivo mutation BMD. The $BMDL_{50}$ calculated for NBP was therefore used in this way to calculate new safe limits.

Table 1 Properties of TGR assay and ecNGS

	TGR assay	ecNGS
Scope of mutation detection	Reporter gene-specific mutations (e.g., *lacZ*, *gpt*)	Genome-wide mutation detection, covering point mutations, insertions, deletions
Throughput	Low	High
Regulatory acceptance	Widely accepted, validated	Not fully validated yet for regulatory use
Test system/ethical considerations	Transgenic rodents	Wild type rodents (or any other species)
Costs	High (breeding and maintenance of transgenic animals, labor-intensive)	Medium (sequencing costs, computational analysis, potential to reduce in cost with time)
Time	Long lead time, globally limited breeding and testing capacities	Shorter lead time, sequencing capacities are currently growing
Data interpretation	Simple, based on a defined number of mutations	Complex, large datasets requiring advanced bioinformatics
Integrable in standard toxicity studies (3Rs)	No	Yes

Consistent with the current trends in the regulatory landscape for NDSRIs, AIs can be supported by quantum–mechanical (QM) modeling that captures the underlying structure–activity relationships (SARs) of in vivo mutagenicity using electronic-structure theory. An appropriate model should satisfy the OECD guidelines for (Q)SARs and conceptually align with the SARs in the CPCA (Cross and Ponting 2021). The CADRE (Computer-Aided Discovery and REdesign) tool was developed for this purpose and was externally validated in a previous study (Kostal and Voutchkova-Kostal 2023). In contrast to the CPCA, which is a rule-based SAR, CADRE uses QM and mixed QM/MM (Quantum and Molecular Mechanics) calculations to relate key events in the nitrosamine metabolism to cancer bioassay data (TD_{50}'s) in a statistical approach. With reactivity metrics assessed from electronic structure, CADRE is accurate outside current knowledge, which is critical when extrapolating from small nitrosamines to the larger and more complex NDSRIs (Kostal and Voutchkova-Kostal 2023). To that end, the CADRE QM tool along with a complementary and fully validated CYP-binding model (Kostal and Voutchkova-Kostal 2025) were leveraged to compare and contrast NBP to the potent NDEA with robust carcinogenicity data. This analysis showcases the value of an integrated in vivo–in silico framework, where the latter offers a highly mechanistic interpretation of the former and thus increases confidence in the proposed AI limit. A predictive QM model can also be invoked a priori to gauge feasibility of a higher AI, before conducting time- and cost-intensive in vivo studies.

In the 28-day in vivo mutagenicity study presented here, for the first time, wild-type female NMRI mice were used. According to OECD TG 488 (Transgenic Rodent Assays), which was the basis for the study design, when only somatic data are needed, which was the case in the present study, such studies could be performed in either sex, since the mutation response is similar between male and female animals (OECD 2022). In the light of the 3Rs and animal welfare, female mice were selected as these can be socialized without stress in groups. In contrast, male mice need to be single-housed, which causes stress and discomfort (Kappel et al. 2017). Mutagenicity in mice was assessed using duplex sequencing followed by BMD modeling and was supplemented by quantum–mechanical and in silico modeling to predict CYP binding and potency of NBP. Furthermore, using BMD analysis, we were able to calculate new safe limits for NBP, which are higher than the published AI of 1.5 µg/person/day. The integrated in vivo–in silico investigation provides a data-based determination of safe limits, suggesting that the AI based on structural considerations only might be over-conservative and should not be capped at the TTC.

Materials and methods

Chemicals

Nitroso-bisoprolol (NBP, CAS#2820170–76-9) and benzo(a)pyrene (BaP, CAS#50-32-8) were purchased from Sigma-Aldrich. Nitroso-dibutylamine (NDBA, CAS #924-16-3) was purchased from SimSon Pharma Limited and 1-Cylopentyl-4-nitrosopiperazine (CPNP, CAS#61379-66-6) from LGC Labor GmbH. Post-mitochondrial S9 fractions from hamsters induced with phenobarbital/benzonaphthoflavone and rats induced with Aroclor™ 1254 as well as uninduced hamster S9 were purchased from MolTox Inc., Boone, NC, USA.

Bacterial reverse mutation tests

Histidine-dependent *Salmonella typhimurium* strains TA98, TA100, TA1535 and TA1537, and tryptophan-dependent *Escherichia coli* strain WP2*uvrA* were used in the Ames test applying the standard and modified (Prival/Mitchell) conditions (OECD 471) and the Enhanced Ames Test (EAT) protocol recommended by European Medicines Agency (EMA) (EMA 2024c). Assay conditions are summarized in Table 2. A detailed description of the procedures and mutation frequencies (yet to be published) can be provided upon request.

To assess treatment-related effects, a fold increase was considered mutagenic if there was a biologically significant increase in the mean number of revertants, exceeding a threshold of twofold (for TA98, TA100, WP2 *uvrA*) or threefold (for TA1535, TA1537), compared to the concurrent negative controls.

Hypoxanthine–guanine-phosphoribosyl-transferase (HPRT) mutation assay in V79 cells

The test was performed as described in the OECD test guideline 476. V79 cells (Technical University, 64,287 Darmstadt, Germany) were cultured in MEM (minimal essential medium) containing Hank's salts, neomycin (5 µg/mL), 10 % FBS, and 1 % amphotericin B at 37 °C in a 1.5% CO_2 humidified atmosphere. Cells were rinsed with PBS, trypsinized, and seeded at a density of approximately 0.7 to 1.2×10^7 in plastic flasks for 24 h to reach 50–70 % confluence before exposure to test substance. For treatment, the medium was replaced without FBS with and without S9 (50 µl/mL) containing NBP, solvent or positive control material. After 4 h treatment, cells were washed with PBS, trypinized, and sub-cultivated at a density of 2×10^6 cells per 175 cm^2 flask. After 3–4 days, cells again were sub-cultivated as described before. After the expression time of 7 days, $4–5 \times 10^5$ cells were seeded in five cell culture flasks

containing 6-thioguanine. Two additional 25 cm^2 flasks were seeded with approximately 500 cells each in non-selective medium to assess viability. After 8 ± 2 days (for viability assessment) and approximately 9 ± 2 days (for mutation analysis), the colonies were stained using 10 % methylene blue in a 0.01 % KOH solution and colonies were scored to determine the overall mutagenicity.

To assess treatment-related effects, a statistical analysis was performed comparing the numbers of mutant colonies counted for the untreated groups with them of the group treated with NBP. To assess a possible dose-dependent increase of mutant frequencies, a linear regression was performed. To evaluate a significant increase of the mutation frequency, a t test was performed. Tests were judged as significant whenever the p value was below 0.05.

Computer-aided discovery and REdesign (CADRE) computational modeling

Quantum–mechanical (QM) calculations

The tiered structure of the CADRE nitrosamine model is an externally validated tool (Kostal and Voutchkova-Kostal 2023), which has been used across industry in support of AI-limit assessment for over 2 years. In contrast to the CPCA or read-across, CADRE relies on the electronic structures of impurities, where quantum–mechanical calculations are used in a statistical model to link key events in nitrosamine mutagenicity with carcinogenic potency. The model assesses ionization and tautomer states of the compound prior to density functional theory (DFT) calculations and uses aqueous Monte Carlo (MC) simulations in conjunction with mixed quantum and classical mechanics calculations (QM/MM) to compute physicochemical properties and solute–solvent energetics (i.e., Coulomb and van der Waals interactions). This enables CADRE to define a biologically relevant conformational landscape and to gauge bioavailability of nitrosamines prior to capturing their reactivity. CADRE estimates reactivity using the QM-FMOT (Frontier Molecular Orbital Theory) approach (Kostal 2018), where global and atom-based steric factors and electronic indices are calculated at the mPW1PW91/MIDIX + level of theory (Kostal and Voutchkova-Kostal 2023). The mPW1PW91/MIDIX + method was developed to assess accurate energies of reaction, barrier heights and electron affinities of large molecules at a reasonable cost (Lynch and Truhlar 2004). The method was shown to yield more accurate hydrogen-abstraction energetics (the presumed rate-determining step in nitrosamines' bioactivation to the diazonium) than the benchmark second-order Møller–Plesset perturbation theory at ca. 20 % of the computational cost (Lynch and Truhlar 2004).

Statistical modeling

CADRE's statistical model uses the R language and environment for statistical computing (version 4.1.2) (Dalgaard 2010) to carry out data analysis, linear regressions and linear discriminant analyses (LDAs). Multivariate normality (mvn) of descriptors is determined using the mvn library; the original descriptor selection is based on a genetic algorithm, as implemented in the library genalg, using 100 iterations with a mutation probability of 0.05 and the Bayesian

Table 2 Summary of assay conditions applied in the bacterial reverse mutation test

	Standard Ames	Modified (Prival/Mitchell) Ames	EAT	Ames screening
Bacterial strains	TA98, TA100, TA1535, TA1537, WP2 *uvr*A			TA100, TA1535, WP2 *uvr*A
S9	10% PB/NF rat (1st and 2nd series)	10% PB/NF rat (Exp. I) 30% uninduced hamster (Exp. II)	30% Aroclor-induced rat 30% induced hamster	30% uninduced hamster S9
Preincubation	60 min (37 ± 2 °C)	30 min (30 °C)	30 min (37 ± 2 °C)	30 min (37 ± 2 °C)
Test item concentrations	5–5000 µg/plate (1st) 50–5000 µg/plate (2nd)	3–5000 µg/plate (Exp. I) 33–5000 µg/plate (Exp. II)	5–5000 µg/plate	5–5000 µg/plate
Test item solvent/volume	DMSO/10 µL	DMSO/100 µL	DMSO/10 µL	DMSO/10 µL
Positive controls -S9	NaN_3 (TA1535, TA100) 4-NOPD (TA1537, TA98) NQO (WP2 *uvrA*)	NaN_3 (TA1535, TA100) 4-NOPD (TA1537, TA98) MMS (WP2 *uvrA*)	NaN_3 (TA1535, TA100) 4-NOPD (TA1537, TA98) NQO (WP2 *uvrA*)	NaN_3 (TA1535, TA100) NQO (WP2 *uvrA*)
Positive controls + S9	2-AA	2-AA (rat and hamster S9) Congo red (hamster S9)	2-AA NDBA 1-CPNP	2-AA NDBA 1-CPNP

Exp Experiment; *-S9* without metabolic activation; *+S9* with metabolic activation; *NaN* Sodium Azide; *4-NOPD* 4-nitro-o-phenylene-diamine; *NQO* 4-Nitroquinoline-N-oxide; *MMS* methyl methane sulfonate; *2-AA* 2-aminoanthracene; *NDBA* N-nitroso-dibutylamine; *1-CPNP* 1-Cyclopentyl-Nitrosopiperazine

Information Criteria (BIC) to avoid overfitting. Internal performance was estimated with the leave-one-out (LOO) cross-validation method, and the final model was selected using performance metrics from external validation (Kostal and Voutchkova-Kostal 2023). The dataset used for model training was obtained from the Lhasa Carcinogenicity Database (LCDB, carcdb.lhasalimited.org). CADRE's LDA models used in this study were trained to i) classify N-nitrosamine contaminants into three potency categories: potent COCs (Cat 1, TD50 ≤ 0.15 mg/kg), COC compounds (Cat 2, 0.15 < TD50 ≤ 1.5 mg/kg), and non-COCs (Cat 3, TD50 > 1.5 mg/kg), and ii) distinguish carcinogens from non-carcinogens. The overall accuracy of the CADRE tool was reported to be 77 % in external testing for the LDA models and > 80 % for the MLR models; CADRE extrapolation to the NDSRI space was explored and found to be reliable (Kostal and Voutchkova-Kostal 2023), owing to the physics-led approach to the model, i.e., its reliance on the underlying chemistry (vs. chemicals in the training set).

CYP-binding evaluation

As NDSRI's ability to bind a CYP P450 in a catalytically optimal pose may be limited by their size, conformational flexibility, or solubility (Buchwald 2014; Cross and Ponting 2021), a complementary model in CADRE assesses CYP binding prior to QM evaluation of NDSRI bioreactivity (Kostal 2024; Kostal and Voutchkova-Kostal 2025). The approach is a multi-docking Monte Carlo search method, based on a broadly applicable and extensively validated method (Buchwald 2014; Cross and Ponting 2021) which identifies binding poses using an induced-fit between the CYP and the substrate, where both the substrate and active-site residue side chains are sampled. Binding scores are computed across 9 isozymes relevant to nitrosamine metabolism (1A1, 2A6, 2B6, 2C8, 2C9, 2C19, 2D6, 2E1 and 3A4) in both the Fe(III) and the Fe(IV) = O states of the P450 catalytic cycle. The proximity of the α-C to the heme's iron is evaluated across all thermodynamically favorable poses, and its impact on the catalytic feasibility is assessed using a well-accepted rule (Durairaj et al. 2019), requiring a catalytically optimal pose within 4 Å between the iron and the α-C in the Fe(III) complex. To ensure catalytic viability is maintained through the P450 cycle, proximity of α-C to the Fe(IV)=O is assessed in parallel simulations, where a distance of less than 3.5 Å is necessary so long as the binding is thermodynamically favorable. Only if both Fe(III) and Fe(IV)=O states predict catalytically feasible binding, the model identifies the NDSRI as potentially active in the CYP. The synthesized outcomes of the CYP model are semaphore-coded, where red implies catalytically optimal pose; orange implies a catalytically competent pose (with lower predicted turnover, based on a 4–6 Å distance in the Fe(III) complex); and green implies no predicted catalytic activity (typically cases where all poses are unfavorable or above 6 Å from iron). The scoring function in CADRE's docking model was identified as the best approach in the last benchmark CASF-2016 (Su et al. 2019), and its search method showed 81 % success rate at reproducing the X-ray pose when evaluated across 800 protein−ligand complexes (Nguyen et al. 2020). The latter is further improved upon in the current implementation within the CADRE tool by considering ten parallel simulations for each NDSRI–CYP complex, resulting in an exhaustive search of the active site (Devaurs et al. 2019).

In life procedures

Study design

The study design followed the recommendations for the in vivo mutagenicity assay conducted in transgenic animals, i.e., OECD TG 488, which is currently considered the gold standard (OECD 2022). To allow a dose–response analysis, five NBP dose groups were included (Fig. 2).

Animals and housing

Female Crl: NMRI (Han) mice were purchased from Charles River, Sulzfeld, Germany. They were group-housed (2 animals/sex) in type III Makrolon® cages with enrichment, and at treatment start, they had an age of 10 weeks and average body weight of 31.8 g (27.9–36.7 g). In accordance with the German Law on the Protection of Animals (Article 8a), the authorities in charge permitted this type of study. The pertaining file at the "Regierungspräsidium Darmstadt" bears the reference" DA4/ 9010".

NBP treatment of NMRI mice

The vehicle, test item, or reference was given by a daily oral administration with a volume of 5 mL/kg body weight via gavage (flexible tube) for 4 weeks. Vehicle consisted of 0.5% Methocel [Methocel K4M Premium Hydroxypropyl Methylcellulose, Colorcon (Dow)] + 0.25 % Tween20 (Merck KGaA) in water (deionized). *N*-Nitroso-Bisoprolol (Sigma-Aldrich, Product Number 51812, batch BCCH5712) was prepared in vehicle by a stirrer for 0.5 h, then ultra-turrax, and again stirred for 0.5 h. The suspension was stored under continuous stirring at room temperature and used for up to 4 days. Benzo[a]pyrene (Sigma-Aldrich, Product Number B1760, batch SLCN8369) was diluted in olive oil (Sigma-Aldrich) and stirred light protected for 0.5 h and kept under room-temperature conditions until the end of each treatment. All formulations were shown to be within the acceptance criteria of ± 15 % recovery for all time points relevant for their use in the study.

Blood sampling for toxicokinetics and clinical pathology

20 µL blood were taken via tail vein at 0.5, 1, 3, 7, and 24 h after the first (at D1) and at 0, 0.5, 1, 7, and 24 h after the last administration from all mice treated with N-nitroso-bisoprolol or at 1 h after the first and the last administration of Benzo[a]pyrene. For hematologic and clinico-chemical examinations 0.4 mL blood were taken sublingually or retrobulbarly under inhalation anesthesia. Further details on simple preparation for bioanalysis or investigated clinical pathology parameters are described under "supplementary data".

In-life outcome measures

Animals were investigated daily for clinical signs, twice per week for body weight changes and once per week for food consumption.

Tissue sampling for duplex sequencing

On study day 31 (3 days after the last dosing) mice were humanely euthanized (CO2) and subjected to a necropsy ensuring a DNase free working area using 10 % bleach (0.6 % sodium hypochlorite solution). To collect bone marrow, both femuri were removed, both ends clipped off, and the cells were rinsed with approximately 250–500 µL of ice-cold sterile PBS (Hank´s Balanced Salt Solution HBSS with calcium and magnesium, without phenol red) into a micro-centrifuge tube. The bone marrow was then centrifuged at 2000 g for 5 min at 4 °C to pellet the cells. The supernatant was aspirated and discarded except for approximately 2 mm of residual PBS above the cell pellet. A piece of liver parenchyma of > 75 mg was excised, washed with PBS, and transferred into a microtube. The tissue was kept cool (on ice) throughout the necropsy and thereafter immediately frozen with liquid nitrogen and stored at -80 °C.

DNA extraction and library creation

Liver tissue and bone marrow cells were thawed and extracted using 25 mg liver tissue and bone marrow cells of both femuri per sample with the Qiagen DNeasy Blood & Tissue Extraction Kit. Purified DNA was eluted in low-EDTA TE buffer, pH 8.0. DNA mass and concentration was tested using the Qubit Flex Fluorometer and Thermo Fisher Qubit dsDNA Quantitation, High Sensitivity kit. DNA integrity for each sample was assessed using Agilent TapeStation 4200 and Agilent High Sensitivity D1000 kits.

Control and Experimental samples were tested with the @@TwinStrand DuplexSeq™ Mouse Mutagenesis Library Preparation Kit for v2 Chemistry, in singlet with 500 ng DNA input to target over 500 million informative duplex bases of data per sample.

For each sample, Duplex Sequencing (DS) libraries were prepared with Duplex-Sequencing Kit Version 2.0 using Enzymatic Fragmentation using the TwinStrand DuplexSeq™ Mouse Mutagenesis panel. Briefly, the library preparation protocol included enzymatic fragmentation of genomic DNA, end-repair, and A-tailing, followed by ligation of DuplexSeq™ adapters containing unique molecular identifiers (UMI). Library conditioning was performed using a mixture of glycosylases to remove damaged DNA prior to amplification. Following indexing PCR, target regions of DNA were enriched by hybrid capture using the DuplexSeq™ Mouse Mutagenesis panel and purified with

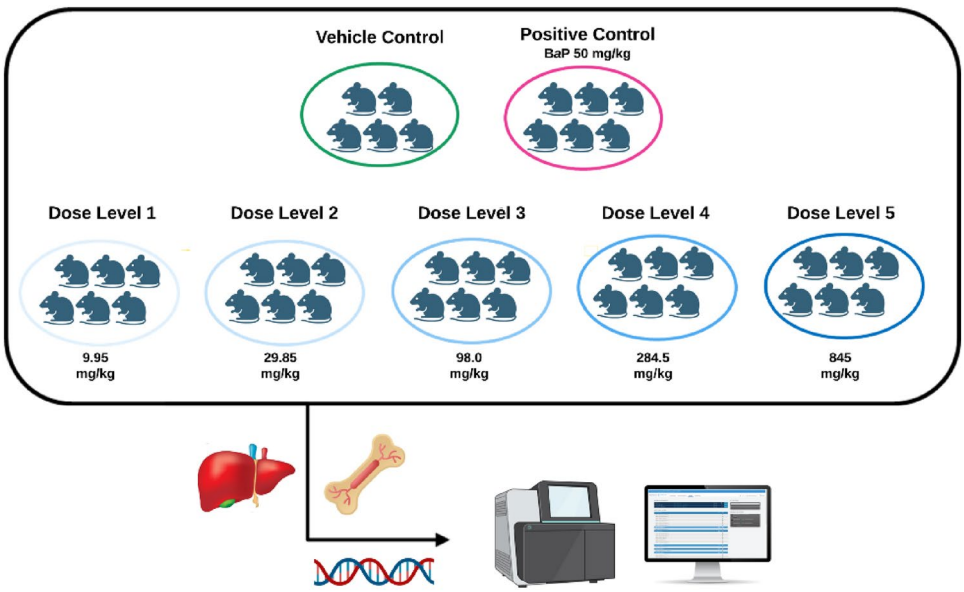

Fig. 2 Design, dose groups, and controls of the 28-day repeated-dose NMRI mouse study from which the tissue samples for duplex sequencing were derived

streptavidin magnetic beads. After washes, additional PCR was performed, followed by another round of hybridization, capture, washes, and a final round of PCR. Final libraries were quantified with Qubit fluorometer, and fragment size was assessed using an Agilent TapeStation system prior to pooling. Libraries were pooled based on the input DNA mass with a maximum of 280 million paired-end reads per library and sequenced using paired-end 150 base pair sequencing on an Illumina NovaSeq 6000 in accordance with SOP-0307 NovaSeq 6000 Sequencer.

Sequencing and data analysis

Duplex sequencing data were generally processed as previously described in Valentine et al. (Valentine et al. 2020) by TwinStrand's production services Duplex-Sequencing Pipeline. In short, raw sequencer-generated basecalls (BCL files) are demultiplexed and an unmapped BAM (uBAM) file is generated for each library. Unique molecular identifiers (UMIs) are extracted from raw reads which are then aligned to the mouse reference genome mm10. Reads having originated from the same source DNA molecule are grouped by UMI and strand-defining elements. Bases with low quality are masked as "N" for ambiguous base assignment. The resulting duplex consensus reads are filtered based on number and quality of reads. Duplex consensus reads undergo interspecies decontamination using Kraken, a k-mer-based taxonomic classifier (Wood and Salzberg 2014), and off-taxa reads are removed. Balanced overlap hard-clipping is performed on read pairs to eliminate biases from double counting bases in overlapping paired-end reads. Variant calling was performed on the duplex consensus BAM using VarDictJava (Lai et al. 2016) with optimized parameters. Variants were annotated using v5 of the Mouse Genomes Project VCF database of known mouse germline variants (Keane et al. 2011).

Prior to performing tertiary analysis, false or inaccurately reported variant calls were filtered from the data by removing overlapping variant calls and variant calls with high percentages (> 80 %) of no-calls.

Per-sample mutation frequency (MF) was calculated using the MFmin method, described in detail in (Dodge et al. 2023). The Student's t test was employed to evaluate the statistical significance of mutation frequency differences between treatment groups within each tissue type.

The simple base substitution spectra and trinucleotide spectra were calculated as previously described in Valentine et al. 2020 (Valentine et al. 2020). Trinucleotide mutational spectra were compared to publicly available signatures in the COSMIC database (Genome: mouse, v3.3.1—accessed May 2023) as well as those published in Kucab et al. 2019 (Kucab et al. 2019).

BMD analysis

NBP liver and BM ecNGS mutation frequency (MF) data were subjected to BMD analysis using PROAST v70.1 (provided by the Dutch National Institute for Public Health and the Environment (RIVM) at https://www.rivm.nl/en/proast) for model averaging, which is currently considered to be the most advanced and precise method for analyzing continuous data (Hardy et al. 2017). Furthermore, the covariate BMD approach was used to increase the precision of the analysis (Wills et al. 2016b), particularly due to the experimental variation at the low doses in the BM dose response. NDEA data were used for covariate analysis due to the similar mutation spectra, mutation mechanism, and use of duplex sequencing with the same sequenced areas of the genome (Bercu et al. 2023).

Permitted daily exposure (PDE)

The ICH Q3C and Q3D guidelines contain the PDE calculation. The PDE can be used if a threshold mechanism can be demonstrated, such as DNA repair. The calculation contains a point of departure metric, namely the NOEL. This can be switched out for the BMDL which is a preferential metric from which to calculate a PDE (Johnson et al. 2021). The BMDL is from the most relevant endpoint, and for mutagenic carcinogens, this can be mutation or cancer. The first step is to correct it to an average human body weight of usually 50 kg for impurities. To account for the uncertainty around this value, a series of uncertainty factors (UFs) are used (ICH 2024). The calculation is done according to the following formula:

$$PDE = \frac{PoD}{combined\ UF} * 50\ kg.$$

Acceptable intake (AI) calculation

Relative potency has been shown for nitrosamines of low and high potency across a range of structures and metabolic and reactive profiles (Wills et al. 2017). This relative potency relationship between in vivo mutation and cancer within the cancer bioassay has been shown using published tumor dose 50 (TD_{50}) metrics from the cancer potency database (CPDB) at Lhasa (LHASA 2024). In vivo mutation data have been generated for seven exemplar nitrosamines with robust carcinogenicity data by industrial partners of the HESI GTTC Mechanism-based Genotoxicity Risk assessment (MGRA) working group using rodent transgenic gene mutation endpoints (TGR), and BMD Confidence Intervals have been calculated (Bercu et al. 2016, 2023; Jolly et al. 2024; Powley et al. 2024). This direct correlation between mutation and cancer for nitrosamines across a range of structures and potencies shows that mutation is a good marker

of cancer potency. The link between the endpoints is that increased mutation leads to increased cancer, as mutations in cancer genes such as tumor suppressor genes to reduce activity, or within proto-oncogenes to increase expression and cell division as oncogenes lead to more cancer. There is therefore correlation and causation between $BMDL_{50}$ and TD_{50} relative potency relationship. These investigations are building work from the HESI GTTC MGRA working group and are yet to be published while also being presented at conferences (e.g., EUROTOX 2024 (Johnson 2024)) and being shared with regulatory bodies (Jolly et al. 2025).

Within the NBP study, ecNGS mutation frequency data has been used to calculate the BMDL values, and these are compared to those from a key comparator compound, i.e., NDEA. The calculation is a simple one that compares the BMDL from the test compound to the anchor compound BMDL to create a relative potency factor, and this factor is then multiplied against the anchor compound AI (Bercu et al. 2016; Zhang et al. 2024) using the following formula:

$$AI = \frac{BMDL\ test\ compound}{BMDL\ anchor\ compound} * AI\ anchor\ compound.$$

Results and discussion

Table 3 summarizes the in vitro and in vivo mutagenicity tests conducted for NBP, including the conditions applied and the corresponding outcomes. Further details are provided in Sect. 3.1 and 3.3, respectively.

In vitro *mutagenicity*

Bacterial reverse mutation assays

In the Standard and Modified Ames tests, no increase in revertant colonies was observed after exposure of the bacteria to NBP. All mean revertant counts were within the historical negative control ranges. No concentration-related increases were observed. In conclusion, NBP was non-mutagenic under these conditions (unpublished data, manuscript in preparation). Following the publication of the recommendation to use the EAT protocol for assessing N-nitrosamines, an additional Ames test was conducted under the specified conditions.

Significant increases in revertant colonies were observed in the presence of 30% hamster S9 for bacterial strains TA100 and TA1535 following exposure to NBP. The additional positive controls, NDBA and 1-CPNP, also induced increases in revertant colonies for the bacterial strains TA100, TA1535, and WP2*uvrA* (Table 4). Using 30 % uninduced hamster S9 in the EAT conditions, no increase in revertant colonies was observed (see supplemental data). In summary, NBP was negative using 10 % and 30 % induced rat or 30 % uninduced hamster S9. In an Enhanced Ames Test (EAT), NBP induced mutation frequencies significantly in the presence of 30 % induced hamster S9 only, confirming that the most stringent conditions of the EAT are appropriate to detect the mutagenic activity of weak mutagens, such as NBP.

In vitro mammalian gene mutation test (HPRT)

NBP was assessed for its potential to induce gene mutations at the HPRT locus using V79 cells of the Chinese hamster. Several publications confirmed the suitability of this test system to detect the mutagenic potential of nitrosamines reliably (Baum et al. 2008; Kuroki et al. 1977; Thielen et al. 2006). NDEA showed a significant increase compared to the solvent control in the presence of S9 mix at 10 mM (42.6 mutant colonies per 10^6 cells), confirming the suitability of the test system for detection of the mutagenic potential of nitrosamines. The solvent control samples showed a spontaneous mutation rate of 7.4 (-S9) and 7.9 (+ S9) mutant colonies per 10^6 cells. NDEA showed a significant increase compared to the solvent control in the presence of S9 mix at 10 mM (42.6 mutant colonies per 10^6 cells). No relevant increases were observed in this in vitro mammalian cell gene mutation assay (HPRT) upon exposure to NBP and thus, NBP was concluded to be non-mutagenic under the conditions reported (Fig. 3).

In silico *analysis*

CADRE QM model of metabolic reactivity

Consistent with experiment, CADRE's QM model predicted NBP as a non-COC impurity ($TD_{50} > 1.5$ mg/kg/day), suggesting an AI above 1,500 ng/day. This result can be interpreted via an electronic-structure read-across (ESRA) to the well-studied NDEA, which is correctly predicted as a potent COC carcinogen in the model's training set. We have reported on the utility of ESRA in our previous study (Kostal and Voutchkova-Kostal 2023) as well as in several collaborative publications that integrate in silico modeling with in vivo assays of NDSRIs (Roper 2025; Zhang et al. 2025). In Table 5, we summarize the key drivers, extracted from the validated QM model for both NBP and NDEA. Our analysis indicates that NBP is less susceptible to radical chemistry and nucleophilic attack at the α-C(s), capturing the initial hydroxylation step and the reactivity of the diazonium metabolite with DNA, respectively. Both properties are computed in CADRE using the Fukui function, $f(r) = \left[\frac{\partial \rho(r)}{\partial N}\right]_{v(r)}$, which measures the propensity of an atom to accept or

Table 3 Summary of in vitro and in vivo mutagenicity testing performed for NBP

Assay	Standard Ames test (OECD 471)*	Modified Ames test (Prival/Mitchell)*	Enhanced Ames test (EMA 2024a, b, c)	HPRT in V79 (OECD 476)	Duplex sequencing in vivo
Conditions	Without S9, 10 % induced rat S9, plate incorporation, 60 min pre-incubation protocol (37 ± 2 °C)	Without S9, 10 % induced rat S9, 30 % uninduced hamster S9 plate incorporation 30 min pre-incubation protocol (30 °C)	Without S9, 30 % induced rat S9, 30 % uninduced hamster S9*, 30 min pre-incubation protocol (37 ± 2 °C)	Without S9, with induced rat S9 (0.75 mg/mL final concentration), 4 h treatment	NMRI mice, 1 × daily treatment (4 weeks), bone marrow and liver, BMD analysis, PDE and AI calculation
Result	Negative	Negative	Positive with 30 % induced hamster S9 *Negative with 30 % uninduced hamster S9	Negative	Positive $BMDL_{50}$ 140 mg/kg bw (BM), $BMDL_{50}$ 96 mg/kg bw (liver)

*Unpublished data

donate electron density, and can inform local reactivity (Kostal and Voutchkova-Kostal 2023; Schieferdecker and Vock 2025; Torrent-Sucarrat et al. 2010; Voutchkova-Kostal et al. 2022; Wondrousch et al. 2010). For radical chemistry, it is defined as $f^0(C_\alpha) = \left[\rho_{N+1}(C_\alpha) + \rho_{N-1}(C_\alpha)\right]/2$, and for electrophilic susceptibility, it is computed as $f^+(C_\alpha) = \left[\rho_{N+1}(C_\alpha) - \rho_N(C_\alpha)\right]$, gauging the change to electron density on the α-C(s) as a result of an external electron-density flux. Normalized using the Hirshfeld Population Analysis (HPA), a maximum in the radical/electrophilic susceptibility corresponds to greater propensity for the process. From Table 5, both metrics indicate greater reactivity of NDEA over NBP. The computed solvent-accessible volume area (SAVA) at the α-C(s) and β-C(s), reflecting steric hindrance in the hydroxylation step, is consistent with our electronic analysis, showing NBP to be less reactive (i.e., more sterically hindered) than NDEA.

Metabolic-reactivity outcomes, deconstructed into electronic and steric drivers, are further supported by computed aqueous solubility metrics and predicted Caco-2 (i.e., apparent Caco-2 cell permeability in nm/sec), which is a model for non-active transport across the gut–blood barrier. The former is derived from energy pair distributions (EDFs) obtained from QM/MM/MC simulations within CADRE, and the latter is predicted from the same simulations in linear-response calculations, as detailed in our previous study (Kostal and Voutchkova-Kostal 2023). These properties indicate that NDEA is less water soluble and thus more bioavailable via oral ingestion than NBP, though both compounds have high predicted permeability rates (i.e., > 100 nm/sec) (Table 5). To that end, we propose that it is primarily lesser reactivity than bioavailability driving the difference in carcinogenic potency of NBP over NDEA.

CADRE CYP-binding panel analysis

In addition to the QM analysis above, the CADRE in silico framework considers CYP binding, which is particularly relevant for larger and/or conformationally rigid NDSRIs (Kostal and Voutchkova-Kostal 2025). While NDEA is readily metabolized by CYPs (primarily by CYP 2E1) due to its small size, NBP is larger (MW = 354 g/mol), suggesting potentially decreased activity based on available qHTS studies on CYPs (Buchwald and Yamashita 2014). From Table 6, which summarizes outcomes of both the QM and CYP models, our docking analysis suggests that catalytically optimal binding can only be achieved in CYP 2A6 and possibly 3A4 (the latter being borderline, provided the distance between the α-C and Fe(IV)=O is at the cut-off value of 3.5 Å, (see Methods). Isozymes 1A1, 2C9, and, to a lesser extent, 2C19 are deemed catalytically competent at a lower turnover due to suboptimal distance between the α-C

Table 4 Fold increase values compared to solvent control applying the EAT conditions

NBP [µg/plate]	Without activation					With 30 % rat S9					With 30 % hamster S9				
	TA 98	TA 100	TA 1535	TA 1537	WP2 *uvrA*	TA 98	TA 100	TA 1535	TA 1537	WP2 *uvrA*	TA 98	TA 100	TA 1535	TA 1537	WP2 *uvrA*
5	0.9	0.9	0.6	1.0	0.6	0.9	0.8	0.9	1.4	0.9	1.0	1.1	1.0	0.8	1.1
15.8	0.9	0.9	0.8	1.0	0.9	1.0	1.0	0.9	1.3	0.9	1.0	1.2	1.5	0.9	1.2
50	1.0	0.8	1.0	0.7	1.2	0.8	0.8	0.9	1.3	0.9	1.1	1.2	2.3	0.8	1.0
158	0.8	0.9	0.8	0.7	1.1	0.9	1.0	0.9	0.8	0.9	1.0	1.7	**5.1**	0.7	0.9
500	0.8	1.0	0.7	0.8	0.8	0.6	0.8	1.2	1.3	0.8	0.9	**2.0**	**9.9**	0.8	1.0
1580	0.8	1.0	0.6	0.9	0.8	0.9	0.8	1.6	1.1	0.8	1.0	**2.5**	**16.1**	0.8	1.1
5000	0.2	0.6	0.6	0.4	0.7	0.6	0.8	1.5	0.7	0.8	1.0	**3.4**	**16.6**	0.6	1.1
Pos. CTR	**9.7**	**5.0**	**22.5**	**18.7**	**33.0**	**12.6**	**5.0**	**8.6**	**3.6**	**2.8**	**72.3**	**30.5**	**4.7**	**10.9**	**16.4**
NDBA	–	–	–	–	–	0.9	**2.3**	**42.6**	1.4	**10.5**	1.0	**10.1**	**81.9**	0.9	**22.9**
1-CPNP	–	–	–	–	–	0.7	**6.3**	**60.3**	1.0	**5.3**	1.1	**13.6**	**117.3**	0.7	**10.0**

Data were obtained without and with metabolic activation (30 %) of induced rat and hamster liver S9 mix in bacterial strains TA98, TA100, TA1535, TA1537, and WP2*uvrA* using the EAT protocol. (Relevant increases are printed in bold. Pos. CTR: positive control)

and Fe(III)/Fe(IV)=O. CYP 2B6, 2C8, 2D6, and 2E1 are predicted to be likely inactive due to poor fit of the substrate within the binding pocket. Given the CADRE in silico workflow suggests at least one catalytically optimal isozyme, the overall classification in Table 6 is guided by the outcomes of the QM (i.e., metabolic-reactivity) model, classifying NBP to be a non-COC impurity.

Interpretation of CADRE in silico outcomes

Overall, the CADRE in silico workflow supports the experimental outcomes presented in this study, suggesting that NBP is a non-COC impurity with an AI above 1,500 ng/day. Due to the scarcity of reliable TD_{50} data, the current implementation of CADRE cannot directly support an AI above this limit, which is why the model should be run in tandem with in vivo studies to extrapolate to a specific, higher AI. The CYP-binding assessment showed that only 2A6 and, to a lesser extent, 3A4 are suitable to accommodate NBP in a catalytically optimal pose. While the relatively large, ubiquitous and promiscuous 3A4 is known to catalyze various types of substrates, the 2A6 isozyme is smaller, with binding site at ca. 59 % of the volume of 3A4's pocket (Kuvek et al. 2024). However, NBP is conformationally flexible, allowing it fold within 2A6's active site in both the Fe(III) and Fe(IV)=O complexes (Fig. 4). This is further supported by Buchwald's analysis (Buchwald and Yamashita 2014), which showed that 1A2 (only ca. 14 % smaller pocket than 2A6) can be readily inhibited by compounds with MW between ca. 250 and 400 g/mol in qHTS dose–response assays. While inhibition of P450-mediated metabolism does not equate to catalytically optimal binding, it does suggest the substrate can fit within with the target's binding pocket. One caveat noted in Fig. 4 is that the transition from the Fe(III) to Fe(IV)=O poses requires conformational rearrangement of the substrate, which necessitates additional residue flexibility within the binding pocket, and may pose an impediment on 2A6's catalytic activity of NBP.

The outcomes of the combined in silico assessment can be reconciled by recognizing that CYP binding precedes any metabolic biotransformations. To that end, we can conservatively argue that NBP's binding criterion is satisfied owing to catalytically optimal poses identified in two isozymes (2A6 and 3A4), and thus, the CADRE QM model should be leaned on to determine NBP's potency and, by extension, AI category. As the QM model predicts low reactivity in the key events of the activation pathway to the diazonium, NBP can be classified as a non-COC compound of low potency. The deconstruction of the CADRE's QM model into individual electronic and steric drivers (see Results) rationalizes this outcome, using metrics obtained from the externally validated CADRE model, and previously used in similar ESRA analyses for NDSRIs (Roper 2025; Zhang et al. 2025).

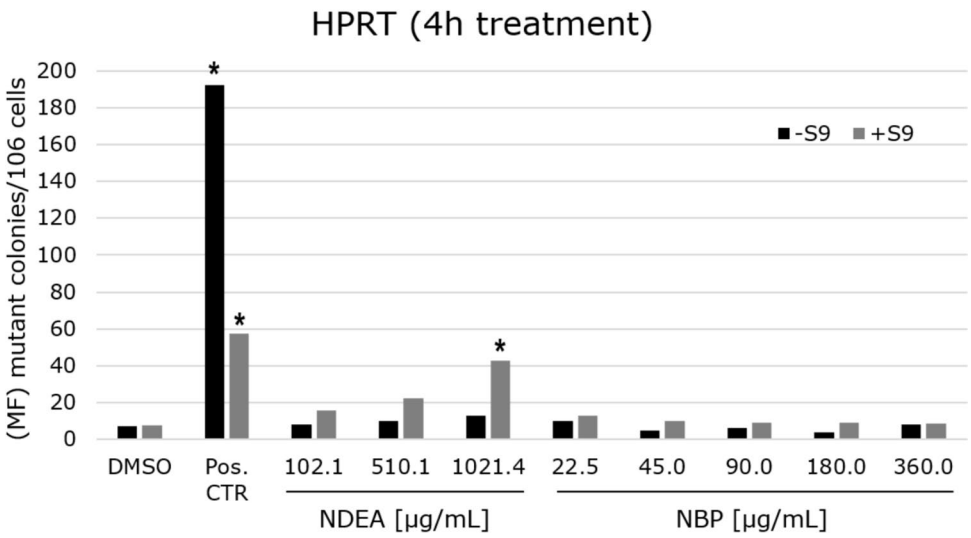

Fig. 3 HPRT gene mutation frequency (number of 6TG resistant clones/106 clone-forming cells) in V79 cells treated for 4 h with NBP, Pos. CTR (positive control) EMS and NDEA compared to solvent control DMSO. Linear regression analysis was used to determine a dose-dependent increase, while a t test was conducted to identify statistically significant increases in mutation frequency at test points exceeding the 95 % confidence interval. N = 2. *$P < 0.05$

Table 5 Electronic, steric, and physicochemical properties of NDEA vs. NBP derived from the CADRE model

	Radical susceptibility	Electrophilic susceptibility	SAVA	$E_{solute\text{-}solvent}$	Caco-2
	(α-C)	(α-C)	α-C/β-C (Å^3)	(kcal/mol)	(nm/sec)
NDEA	0.032	0.041	20.4/34.6	− 31.3	521.8
NBP	0.009	0.014	18.0/14.3	− 89.7	246.3

Electronic, steric, and physicochemical properties computed for NDEA and NBP used to explain the difference in predicted potency categories. Maximal radical susceptibility at the α-C=; Maximal electrophilic susceptibility at the α-C=; SAVA = solvent-accessible volume area; SAVA = solvent-accessible volume area; Esolute-solvent = ECoul + ELJ, i.e., a sum of Coulomb and Lennard–Jones (van der Waals) energetics between the nitrosamine and surrounding water molecules obtained from energy pair distributions in QM/MM/MC simulations; Caco-2 = apparent Caco-2 cell permeability

In vivo *investigations*

Tolerability of NBP in mice

NPB was administered orally and daily by gavage at 9.95, 29.85, 98, 284.5, and 845 mg/kg/d for 4 weeks to NMRI mice. Treatment-related mortality, clinical signs, or change in body weight and food consumption were not observed up to the highest dose of 845 mg/kg/d NBP. Also, the treatment with the positive reference benzo[a]pyrene was well tolerated.

At day 31, 3 days after the last NBP administration, mice were sacrificed for tissue collection and peripheral blood was taken for clinical pathological investigations. Hematology and clinical chemistry revealed no treatment-related alterations neither with NPB up to the highest dose nor with BaP. More details on the in vivo tolerability results can be made available upon request.

Toxicokinetic investigation in NBP treated mice

Toxicokinetic analysis revealed that the Area under Curve $(AUC)_{0\text{-}24\,h}$ and maximal concentration (C_{max}) increased over the dosing range between 9.95 and 845 mg/kg/d, on Day 1 and Day 28. From 9.95 to 29.85 mg/kg/d, the increases were more than dose proportional, from 29.85 to 98.0 mg/kg/d the increases were approximately dose proportional for C_{max} and more than dose proportional for $AUC_{0\text{-}24\,h}$, from 98.0 to 284.5 mg/kg/d, the increases were considered approximately dose proportional for C_{max} on Day 1 and $AUC_{0\text{-}24\,h}$ on Day 28, less than dose proportional for C_{max} on Day 28 and more than dose proportional for $AUC_{0\text{-}24\,h}$ on Day 28. From 284.5 to 845 mg/kg/d, the increases were considered less than dose proportional for C_{max} on Day 1 indicating that a plateau has nearly been reached and approximately dose proportional for C_{max} on Day 28 and $AUC_{0\text{-}24\,h}$ on Day 1 and Day 28. It was confirmed that all negative control animals were not exposed to NBP, and all reference control animals were exposed to Benzo[a]pyrene. The t_{max} was observed at 0.5 h post-dose on most occasions. More details on the toxicokinetic results can be made available upon request.

Duplex sequencing

Mutation sequence data provide information on the types of mutation induced by test substances and their metabolites. The types of mutation are specific to the type of DNA adduct that are being induced, and these adducts are repaired by different DNA repair pathways. The predominant mutagenic DNA adducts induced by N-nitrosamines are the O6-alkyl-G and O4-alkyl-T, and these are repaired by MGMT (Bercu

Table 6 CYP-binding analysis and QM-model summary for NBP

P450 binding summary (NBP)									QM summary (NBP)
1A1	2A6	2B6	2C8	2C9	2C19	2D6	2E1	3A4	
Binding affinity in Fe(III) (kcal/mol)									Predicted TD_{50}
− 7.4	− 6.7	− 6.5	− 6.3	− 6.1	− 6.2	− 6.2	− 2.5	− 6.7	> 1.5 mg/kg/day
Minimum Fe(III)—C_a distance in bound states (Å)									AD score
4.3	3.0	5.4	6.1	5.3	4.9	6.0	3.8	3.6	2+3
Minimum Fe(IV)=O—C_a distance in bound states (Å)									Overall classification
3.4	3.2	3.7	3.9	3.9	3.5	4.1	3.9	3.5	Non-COC

CYP model: red = catalytically optimal (thermodynamically favorable binding in the Fe(III) complex, Fe(III)—Ca within 4.0 Å and Fe(IV) = O—Ca within 3.5 Å), orange = catalytically competent (thermodynamically favorable binding in the Fe(III) complex, Fe(III)—Ca within 6.0 Å and Fe(IV) = O—Ca within 3.5 Å), green = catalytically inactive (thermodynamically favorable binding in the Fe(III) complex, Fe(III)—Ca above 6.0 Å and Fe(IV) = O—Ca above 3.5 Å, or thermodynamically unfavorable binding across all sampled poses). QM model: red = potent COC compounds (Cat 1, TD50 ≤ 0.15 mg/kg), orange = COC compounds (Cat 2, 0.15 < TD50 ≤ 1.5 mg/kg), green = non-COC compounds (Cat 3, TD50 > 1.5 mg/kg) (Bercu et al. 2024). AD Score = applicability-domain score, reflecting confidence in the prediction based on values of computed descriptors relative to the model's training set (2 + 3 = maximum confidence in the calculated metrics and predicted category fully within the models AD (Kostal and Voutchkova-Kostal 2023)

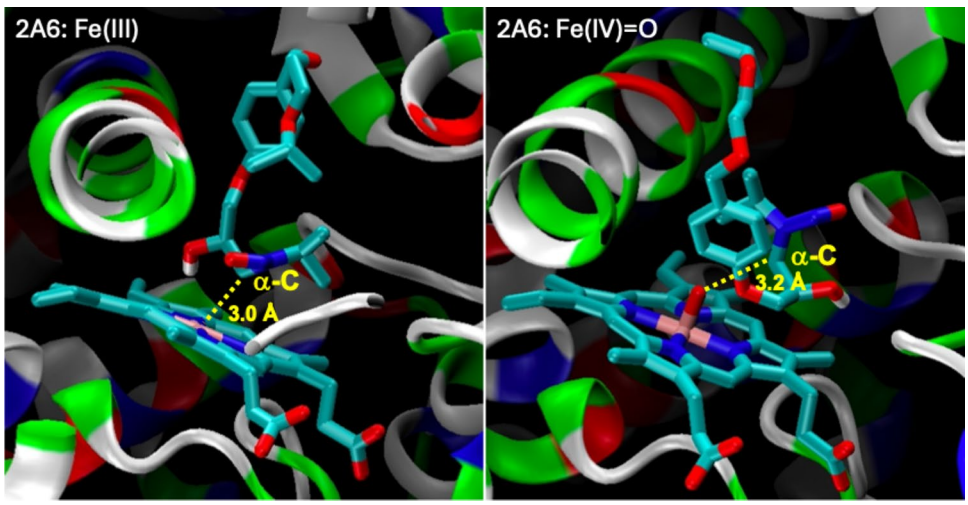

Fig. 4 Snapshots of the best CYP-binding poses of NBP in 2A6 isozyme in the Fe(III) complex (left) and Fe(IV)=O complex (right). Distance to the hydroxylable α-C is shown in yellow dashed line

et al. 2016, 2023; Fahrer et al. 2015). Therefore, in addition to the mutation dose–response information gained from the in vivo ecNGS experiments in mice and ability to define an NOEL and/or BMDL, information is also provided on the mutation, the DNA adduct and the DNA repair pathway. Furthermore, the mutation spectrum is provided for each dose, and due the sensitivity of the approach being in line with the background mutation frequency in the human genome (1 mutation per 100 million base pairs, $MF = 1 \times 10^{-8}$), ecNGS mutagenicity analysis is sensitive enough to accurately assess whether the mutation spectra are the same at low doses of mutagenic exposure as it is at the negative control.

If there is no difference between mutation spectra at the vehicle control and low dose/s of nitrosamines, this provides further support for a threshold mechanism of DNA repair withstanding low levels of these DNA adducts through MGMT repair, as well as providing the BMDL with which a PDE can be calculated, or the BMDL could be used for other risk assessment purposes (Johnson et al. 2021).

Female NMRI (wild-type) mice were treated with daily oral doses of vehicle (negative control), 9.95, 29.85, 98, 284.5, and 845 mg NBP/kg bw for 28 days (n = 6). As a positive control, benzo(a)pyrene (BaP), a pro-mutagen requiring metabolic activation was administered at 50 mg/kg bw for 28 days (n = 5). The animals were sacrificed 3 days after the last administration and liver and bone marrow samples were taken and subjected to duplex sequencing (DS), to investigate mutation frequencies and mutation spectra.

Data quality

Targets were sequenced to an average duplex consensus sequence depth of 15,872 × yielding a mean number of 979 million informative duplex bases per sample. The targeted minimum of 500 million informative duplex consensus bases was achieved for all samples (Fig. 5).

Mutation frequencies Mutation frequencies (MF) were calculated for each sample using the MF_{min} method by dividing the number of identified unique mutant duplex bases by the total number of duplex bases sequenced. If mutations appeared more than once in the same animal, these were considered to be derived from a clonal expansion event and were counted only once. Hence, only independent somatic mutations were taken into account for the MF calculation. Individual mutation frequencies are provided in the supplemental information. The mean MF per dose group are presented in Table 7:

The positive control BaP showed the expected increase in mutation frequencies in both tissues. In both bone marrow and liver, moderate, but statistically significant and dose-dependent increases in mutation frequencies induced by NBP were observed, starting at doses of 29.85 or 98 mg/kg bw, respectively (Fig. 6). The highest inductions of mutation frequency observed were 2.4-fold in the bone marrow and 4.17-fold in the liver, both at the highest NBP dose applied (845 mg/kg bw/d). Of note, variations between individual animals of a dose group were very small, leading to statistical significances at 1.33-fold (bone marrow) or 1.45-fold (liver) relative to the negative control, emphasizing the high sensitivity of the method and consistency of results (Fig. 6).

As the study presented in this manuscript was the first in vivo mutagenicity study conducted in wild-type NMRI, no historical control data are available for this strain. However, there are publicly available MF data for vehicle controls in transgenic mice that range from 4.8×10^{-8} to 5.3×10^{-8} in the liver and 4.1×10^{-8} to 13×10^{-8} in the bone marrow (Dodge et al. 2023; LeBlanc et al. 2022; Schuster et al. 2024; Zhang et al. 2024). A summary of NMRI and published DS mutation frequency data for vehicle controls is shown in Table 8. The data show a high similarity of vehicle control MF in NMRI and transgenic mice. In addition, in the Lhasa Vitic Complex Nitrosamines database (VCN), 20 data sets are reported for DS with BigBlue® mouse with MF in the negative controls in the liver ranging from 3.4 to 9.9×10^{-8} (Lhasa Limited 2025).

Only few historical control data are reported for kidney, but mean values are in the same range as for liver or bone marrow (Zhang et al. 2025). Mutation frequencies observed for 50 mg/kg bw BaP are in line with published data (LeBlanc et al. 2022). Furthermore, when comparing the BaP responses to the vehicle control between the present study with NMRI mice and MutaMouse data from LeBlanc (LeBlanc et al. 2022), it was stronger in the NMRI mice, confirming that this strain is at least as susceptible to mutations as MutaMouse animals (Table 9).

These data show that there are no significant differences in the baseline mutation frequencies between wild-type and transgenic mice. As more in vivo mutagenicity studies in wild-type animals will be conducted, historical control database will gradually be built and expand over time.

Mutation spectra

A lot of information is provided through analysis of changes in mutation spectra following treatment with genotoxic chemicals. For example, if the main mutagenic adduct is considered to be an alkyl group, then one can link the mutation spectrum to the DNA adduct type, and this also provides information on the predominant DNA repair pathway for that adduct (Table 10).

Analysis of mutation spectra of NBP compared to those of other nitrosamines also suggests a threshold mechanism for the DNA repair of NBP-induced mutations by base excision repair (BER) via methylguanine-methyltransferase (MGMT).

Benzo[a]pyrene (BaP) is a well-known environmental pollutant, mutagen, and pro-carcinogen. BaP is metabolized by enzymes like CYP1A1 and CYP1B1, which convert it into its ultimate carcinogenic form, benzo[a]pyrene-7,8-diol-9,10-epoxide (BPDE). This metabolite can form DNA adducts, leading to mutations and potentially cancer (Shiizaki et al. 2017). The liver's high metabolic activity makes it a primary site for BaP activation and subsequent DNA damage. In bone marrow, BaP-induced mutagenesis has been studied using high-accuracy sequencing technologies like Duplex Sequencing (DS). Research has shown that BaP exposure leads to a dose-dependent increase in mutations, particularly in heterochromatic and intergenic regions (LeBlanc et al. 2022). The mutation spectrum in

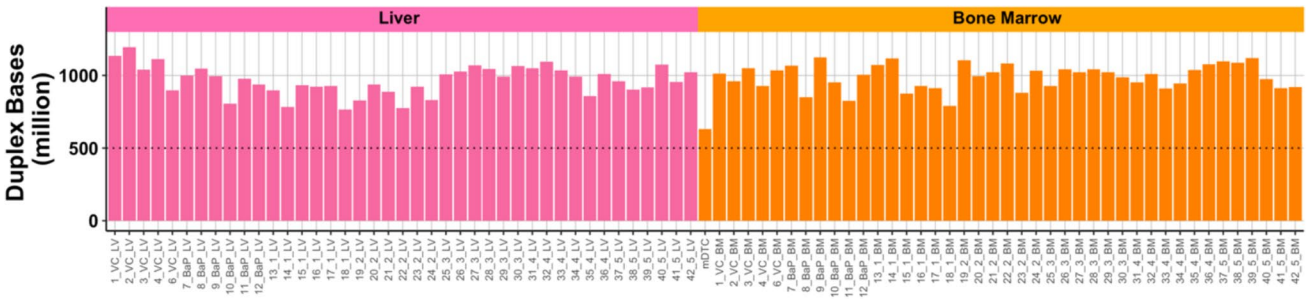

Fig. 5 Duplex sequencing data yield and input mass per sample. The number informative duplex bases generated per sample are represented by the colored bars in millions of duplex bases (y-axis). This metric provides a quantification of the amount of duplex sequencing data output that can be used for assessing mutation frequency. The dashed line shows the targeted minimum of 500 million informative duplex bases

Table 7 Liver and BM mean mutant frequencies

Tissue	Compound	Dose mg/kg/day	MFx10^{-8} Mean	MFx10^{-8} STD	Adjusted *p* value
Liver	VC	0	9.63	2.13	–
Liver	NBP	9.95	10.5	3.92	0.3569
Liver	NBP	29.85	10.0	2.38	0.5229
Liver	NBP	98	14.0	2.39	8.27×10^{-9}
Liver	NBP	284.5	16.7	0.94	3.94×10^{-19}
Liver	NBP	845	40.2	7.09	1.63×10^{-172}
Liver	BaP	50	26.0	3.51	1.18×10^{-70}
BM	VC	0	6.18	1.44	–
BM	NBP	9.95	5.64	1.28	0.48
BM	NBP	29.85	8.19	1.94	0.0009
BM	NBP	98	9.27	1.33	3.75×10^{-7}
BM	NBP	284.5	12.1	2.59	3.68×10^{-18}
BM	NBP	845	14.8	1.46	1.12×10^{-33}
BM	BaP	50	118	8.88	$<2.22\times10^{-308}$

bone marrow often includes C:G > A:T transversions, which are characteristic of BaP mutagenesis (LeBlanc et al. 2022).

NBP ecNGS mutation spectra had a predominance of C > T and T > G mutations (Fig. 7). These are comparable to the mutation spectra from N-Nitrosodiethylamine (NDEA) (Bercu et al. 2023) and N-nitrosopyrrolidine (NPYR) (Fahrer and Christmann 2023; Guttenplan 1990), and could be described as the mutation fingerprint of these substances (Table 11). These mutations are due to NBP inducing alkylation at the O^6-Guanine and O^4-Thymine, which are mis-recognized during replication. These lesions can be repaired by methylguanine-methyltransferase (MGMT) and are the most relevant mutagenic lesion accounting for the mutagenic and carcinogenic potency of nitrosamines (Fahrer and Christmann 2023).

Although there is a similarity in mutation spectra between NBP, NDEA, and NPYR (Kucab et al. 2019), there is a difference in mutagenic and carcinogenic potency between these substances. NDEA is a small nitrosamine that is very potent due to the simple metabolic profile and reactivity of the substance, whereas the larger NPYR and NBP nitrosamines have more complex metabolic profiles, with different steric hindrance and/or the chemical reactivity of the diazonium ion resulting in fewer adducts at the O^6-G and O^4-T regions of DNA, therefore having lower mutagenic potency.

Bercu et al. (2023) and Zhang et al. (2024) have investigated ecNGS dose–response mutation spectra from NDEA in rats and mice. Their investigations showed that at the lower doses, the mutation spectra do not differ from the vehicle control, it also shows that NDEA induced O^6-alkyl-guanine and O^4-alkyl-thymine. This mutation spectra/fingerprint has some similarities to within the mouse liver following exposure to NBP (Fig. 7, Table 11). NPYR was also shown to include C > T and T > A mutations (Kucab et al. 2019), with

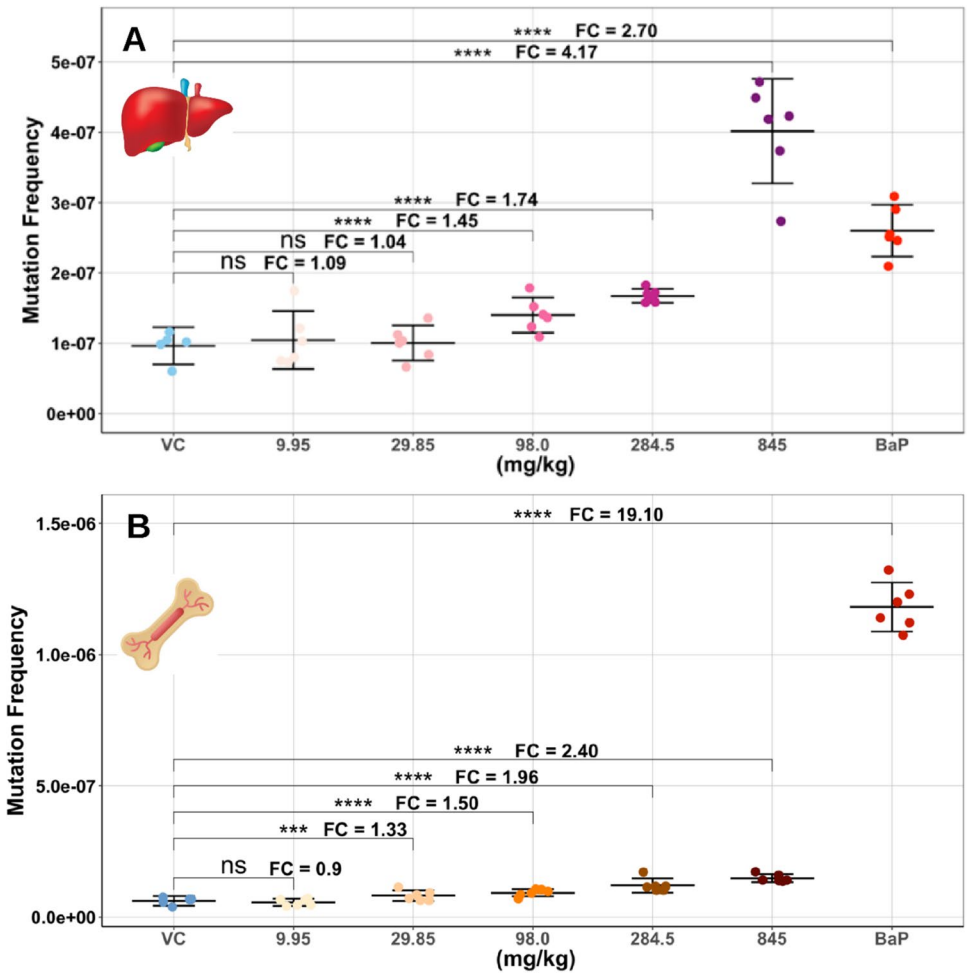

Fig. 6 Mean mutation frequencies induced by NBP in the liver (top) and bone marrow (bottom) of mice treated for 28 days. FC: Fold induction relative to the vehicle control. ****$p < 0.0001$, ***$p < 0.001$, **$p < 0.01$, *$p < 0.05$, ns $p > 0.05$

Table 8 Mutation frequencies in vehicle controls in NMRI and transgenic mice

Mouse strain	MF[a] vehicle (liver) ($\times 10^{-8}$)		MF[a] vehicle (bone marrow) ($\times 10^{-8}$)		References
	MF (mean)	MF (SD)	MF (mean)	MF (SD)	
NMRI wt mice (f)	9.63	2.13	6.18	1.44	Brenneis (2024)
MutaMouse (m)	–	–	13	2.5	LeBlanc (2022)
MutaMouse (m)	–	–	13.1	0.7	Dodge (2023)
MutaMouse (m)	5.33	1.01	4.13	0.45	Schuster (2024)
BigBlue mouse (m)	4.8	0.9	4.9	0.6	Zhang (2024)
BigBlue mouse (m)	4.7	1.1	–	–	Zhang (2025)

[a]Mutation frequency

Table 9 Mutation frequencies in BaP positive controls in NMRI and transgenic mice

Mouse strain	MF ($\times 10^{-8}$) Benzo(a)pyrene (BaP) (50 mg/kg bw/d)				References
	MF liver ± SD	FI[b]	MF bm ± SD	FI[b]	
NMRI wt mice	26 ± 2.13	2.7	118 ± 8.88	19.1	Brenneis (2024)
MutaMouse	–		104 ± 7	8	LeBlanc (2022)

[a]Mutation frequency

[b]FI: fold induction compared to vehicle control

the T > A through O^2-alkylthymine and C > A through reactive oxygen species (ROS) secondary mechanism at 8-oxo-G (Table 6). The similarity in mutation spectra shows that NBP induces mutations are induced in a comparable manner to those of NDEA and indeed most other N-Nitrosamines sequenced to date (Fahrer and Christmann 2023). Furthermore, there is no change in mutation spectra at the lowest doses of NBP at 9.95 and 29.85 mg/kg/kg and potentially 98 mg/kg/day, which supports a threshold mechanism for NBP.

An additional point of interest is that at higher doses, NDEA induces more C > T than T > A mutations, showing that mutagenic adduct O^4-alkyl-Thymine becomes more dominant, where MGMT/AGT could be less efficient at repairing O^4-alkyl-Thymine than O^6-alkyl-Guanine (Bercu et al. 2023). For NBP, there is a similar increase in each mutation.

As there is a predominance of C > T, T > A, and T > C mutations, this supports an MGMT DNA repair mechanism as well as BER (Table 6), this is further shown by no change in mutation spectra at the low doses, and together this argument shows that the ICH statements around PDE being used when a threshold mechanism is shown, is entirely supported here.

Trinucleotide mutation spectra were compared across tissue type and treatment group. In liver, low-dose TA treatment groups (29.85 or lower mg/kg) have similar trinucleotide spectra to the VC group. High-dose TA treatment groups (98.0 or higher mg/kg) have distinct trinucleotide spectra with enriched C > T, T > A, T > C, and T > G mutations (Fig. 8). In bone marrow, no TA treatment group has a distinct trinucleotide spectrum from the VC group. The BaP treated groups have distinct spectra in both tissues (Fig. 8). The spectra have high correlations with known signatures of BaP (Fig. 8).

Benchmark dose (BMD) analysis

In the present study, the covariate BMD approach was used to increase the precision of the analysis as described by Wills (Wills et al. 2016b), particularly due to the experimental variation at the low NBP bone marrow response. The covariate BMD approach allows for fitting a dose–response model to datasets that may differ in background response, or in potency, but have similar shapes. Combining similar datasets may result in a significant improvement in precision (Wills et al. 2016b). Covariate BMD analysis was used for the bone marrow NBP data, as the data set included an MF response lower than the vehicle control, and the MF response at the higher doses was not very large (< 2.5-fold). These data were not optimum for BMD analysis, and inclusion of information of shape parameters from another data set was preferable (Johnson 2025).

Although the liver NBP data were suitable for the calculation of precise BMD confidence interval, and the results were being compared to those from the bone marrow NBP BMD analysis, a covariate BMD approach was considered a like-for-like approach.

Calculations of BMD with or without covariates were conducted and showed that there were no significant differences between BMD values using both rat and mouse data or mice data only as covariate data sets (Table 12 and supplemental information).

There were differences in the BMD values for the bone marrow when using covariate or non-covariate approach. Without covariate analysis, bone marrow seems to produce a lower BMDL, which is an artifact due to the first dose having MF below the background and the highest fold induction of 2.4-fold. For such data sets, covariate BMD analysis is preferred as it increases the precision considerably. Based on these considerations, the covariate BMD approach combining similar data sets is suitable and appropriate for the calculation of NBP BMD confidence intervals (Johnson 2025).

The BMD analysis shows that the dose–response curves of NDEA in rats and mice are very similar with similar confidence intervals (Fig. 9). In contrast, dose–response curves of NBP are distinct from NDEA and there is no overlap of the confidence intervals. Comparing the $BDML_{50}$ of NDEA (0.04 mg/kg bw/day, (Bercu et al. 2023)) to NBP (96 mg/kg bw/day), it could be shown that the NBP $BMDL_{50}$ is three orders of magnitude higher than that of NDEA, suggesting a significantly lower mutagenic potency of NBP. This supports the assumption that NBP does not belong to the highly potent cohort-of-concern nitrosamines.

Table 10 Mutation spectra, underlying adducts and repair pathways

Mutations	G > T/C > A	G > A/C > T	T > C/A > G	T > A/A > T	Apurinic sites
Adducts	8-oxo-G, ROS	O^6-alkylguanine	O^4-alkylthymine	O^2-alkylthymine	N7-dG and N3-dA
DNA repair pathway	Glycosylase recognition with BER	MGMT/AGT	MGMT/AGT	Glycosylase recognition with BER; TLS	Glycosylase recognition with BER; TLS

Mutation spectra and the underlying alkylating adducts that could result in these, according to (Jenkins et al. 2005; Kucab et al. 2019). Information about the predominant DNA repair pathway for that specific DNA adduct is also provided

BER base excisions repair; *MGMT* methylguanine-methyltransferase; *AGT* alkylguanine transferase; *TLS* translesion synthesis

Determination of safe limits using the $BMDL_{50}$ as PoD for PDE and AI calculation

Generally, there are two options to determine acceptable limits for lifetime daily exposure to an impurity. The ICH M7 states that for mutagenic impurities, when a 'threshold mechanism' can be defined, a permitted daily exposure (PDE) calculation can be used. This approach uses a Point of Departure (PoD) metric, namely the NO(A)EL, which can be replaced by the BMDL. To account for uncertainties related to this value, several uncertainty factors are applied, such as e.g., intra- and interspecies variability, study duration, severity of effects, and type of PoD. In addition, a correction to an average human standard body weight of 50 kg is used (Table 13).

The applicability of this approach was also discussed within a Health and Environmental Sciences Institute (HESI) Genetic Toxicology Technical Committee (GTTC) publication (Johnson et al. 2021). For some nitrosamines such as nitroso-diethylamine (NDEA), the type of mutations induced has been already described and mutation spectra have been published. The DNA repair pathways via methylguanine-methyltransferase (MGMT) are well described and considered threshold mechanisms, supporting the applicability to nitrosamines (Fahrer and Christmann 2023; Fahrer et al. 2015). Following this approach and under consideration of a combined uncertainty factor of 12,000 [interspecies extrapolation (F1 = 12 (mice to human)], intraspecies variation (F2 = 10 (general population), study duration (F3 = 10 (< 3 months)), severity of effect [F4 = 10 (mutation considered a severe effect)] and point of departure (PoD) available [F5 = 1 (BMDL superior to NOEL)] and using the BMDL of 96 mg/kg bw/day from the most sensitive tissue, i.e., the liver, a PDE for NBP was calculated as follows (Johnson 2025):

$$\begin{aligned} PDE(NBP) &= \frac{BMDL}{F1 * F2 * F3 * F4 * F5} * 50\ \text{kg} \\ &= \frac{96 \frac{mg}{kgbw/day}}{12,000 * day} * 50\ \text{kg} \\ &= 400\ \mu\text{g/person/day}. \end{aligned}$$

The second option is based on the ICH M7 framework calculating Acceptable Intake (AI) limits based on TD_{50} values derived from carcinogenicity bioassays (ICH 2023). The AI calculated based on the TD_{50} from carcinogenicity bioassays reflects a theoretical additional cancer risk of 1 in 100,000 and applies a linear extrapolation to human. Mutagenicity is the key event for the carcinogenicity of nitrosamines. The high correlation between in vivo mutation and carcinogenicity has been recently shown for seven exemplar nitrosamines of various structural classes with robust carcinogenicity data in the HESI GTTC MGRA working group. Namely, NDMA, NDEA, NPIP, NMOR, NNK, NPYR, and NDELA were assessed in TGR OECD 488 assays using transgenic rats or mice (Johnson 2024; Jolly et al. 2024, 2025) and BMD confidence intervals calculated. Comparison of the in vivo carcinogenic potency based on TD_{50} values and in vivo mutagenicity potency based on $BMDL_{50}$ calculated from TGR mutation data revealed a high correlation ($R^2 = 0.95$), validating the use of in vivo mutagenicity data for the prediction of carcinogenicity potency of nitrosamines (Johnson 2024; Jolly et al. 2025). Thus, the calculation of an AI for an NDSRI using the relative potency of in vivo mutation $BMDL_{50}$ compared to an AI of a known anchor nitrosamine derived from in vivo cancer bioassay data is a scientifically valid approach (Jolly et al. 2024; Powley et al. 2024). This relative potency approach enables the calculation of an AI limit for NBP using the in vivo mutation $BMDL_{50}$ calculated for N-nitroso-bisoprolol (target) and an anchor compound (NDEA) and the AI of this anchor compound (Johnson 2024, 2025; Jolly et al. 2025).

An AI using the NBP $BMDL_{50}$ of 96 mg/kg bw/day and the NDEA $BMDL_{50}$ of 0.04 mg/kg bw/day was calculated as follows:

$$\begin{aligned} AI(NBP) &= \frac{96 \frac{mg}{kgbw/day}}{0.04 \frac{mg}{kgbw/day}} * 26.5 \frac{ng}{day} \\ &= 63,600\ \text{ng/person/day} \\ &\approx 64\ \mu g\text{/person/day}. \end{aligned}$$

We evaluated alternative anchor nitrosamines to determine their influence on the calculated Acceptable Intake (AI) for NBP (Table 14). Zhang et al. recently published a comparative investigation on re-evaluating the AI of NMOR and N-nitroso-reboxetine (Zhang et al. 2025) by comparing mutagenic potencies assessed in TGR studies with a duplex sequencing readout. For both molecules, EMA has published an AI of 127 ng/day, using NMOR for read-across to N-nitroso-reboxetine (EMA 2024b). For N-Nitroso-Reboxetine and NMOR, $BMDL_{50}$ values of 4.49 mg/kg bw/day and 0.024 mg/kg bw/day were derived, respectively. Using the AI of 127 ng/day of the well-studied molecule NMOR as anchor compound, an AI of 24,000 ng/day could be calculated for N-Nitroso-Reboxetine. Based

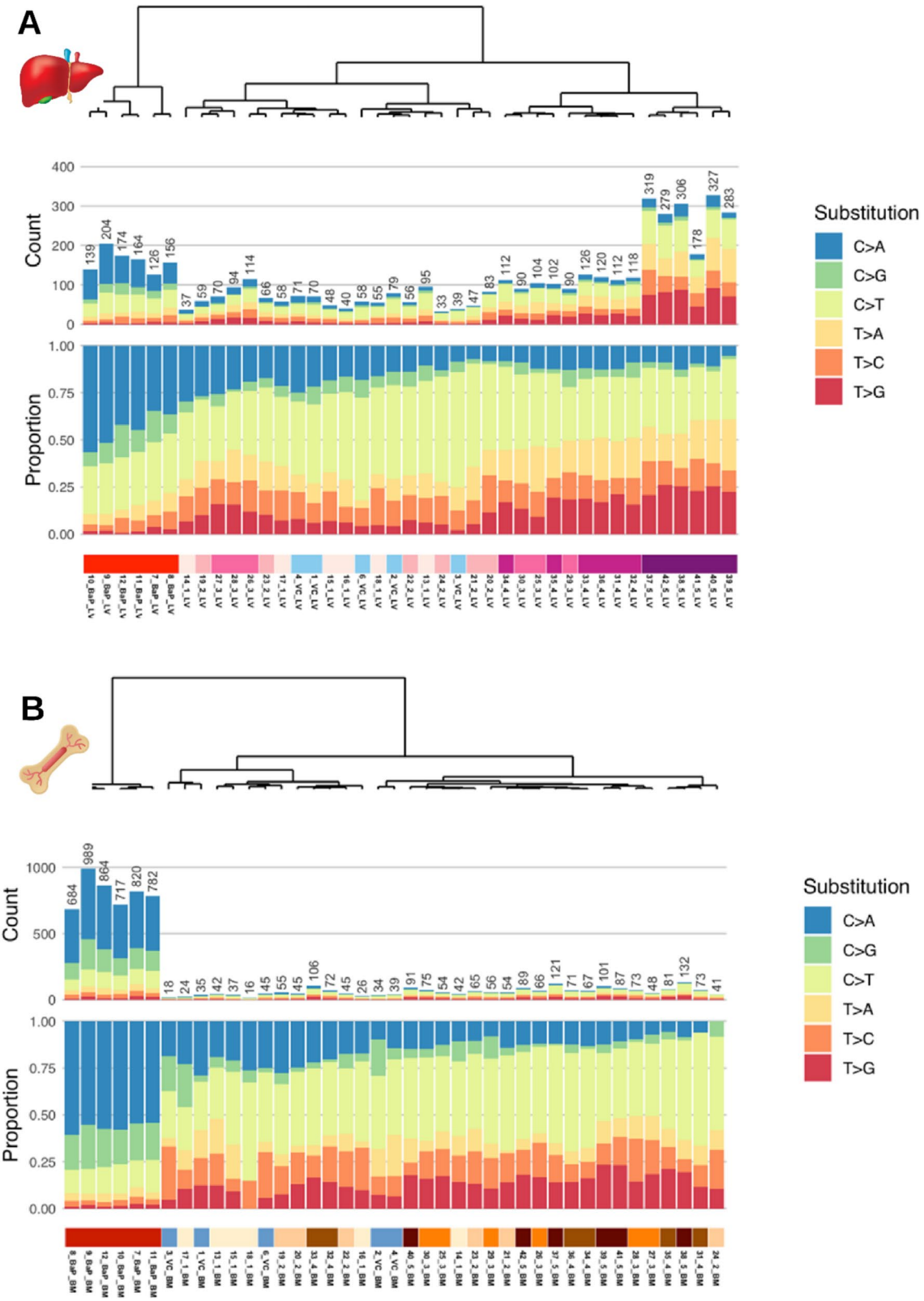
A
Count
Proportion
Substitution
C>A
C>G
C>T
T>A
T>C
T>G
B
Count
Proportion
Substitution
C>A
C>G
C>T
T>A
T>C
T>G

◂**Fig. 7** N-nitroso-bisoprolol (NBP) liver (top) and bone marrow (bottom) mutation spectra from ecNGS. Liver and bone marrow simple base substitution spectra by sample. Unsupervised hierarchical clustering was used to group samples with similar spectra into clusters in the above plot. Clustering is performed using the cosine similarity matrix calculated on base substitution type proportions using the Ward clustering algorithm. The Ward clustering algorithm includes Ward's clustering criterion which squares dissimilarities before cluster updating [described in (Murtagh and Legendre 2014)]. Numbers above bars report the variant counts, which are limited to single-nucleotide variants. The horizontal color bars indicate treatment group. BaP: Benzo(a)pyrene positive control; VC: vehicle control; 1: 9.95; 2: 29.85; 3: 98; 4: 284.5; 5: 845 mg/kg/day NBP

on these results, it was postulated that N-Nitroso-Reboxetine has a far lower mutagenic potency compared to NMOR and that the AI of 127 ng/day might be over-predictive (Zhang et al. 2025).

Applying NMOR as an alternative primary anchor compound, the AI for NBP is increased nearly eightfold to 508 µg/day (Table 14). Additionally, we assessed N-Nitroso-Reboxetine as secondary anchor nitrosamine. This analysis yielded an AI value for NBP of 513 ng/day, very similar to the AI derived with NMOR as primary anchor nitrosamine and eightfold higher than the AI calculated using NDEA (64 µg/day) (Table 14).

Given the additional uncertainty associated with secondary anchor mutation data, we consider the AI based on extrapolation from primary anchors such as NDEA or NMOR to be more robust and thus preferable. Furthermore, using NDEA as anchor yielded the lowest and thus most conservative AI (Table 14).

Hence, lifetime PDE and AI limits of 400 µg/person/day and 64 µg/person/day could be established, which are far above the published NBP AI of 1.5 µg/person/day based on CPCA. This suggests that the current CPCA framework may be over-conservative in certain cases and that a cap for nitrosamine AIs at 1.5 µg/day is not justified.

Conclusions

With this paper, we provide a comprehensive in vitro assessment and the first publication of in vivo data for the nitrosamine drug substance-related impurity (NDSRI) of a β-blocker. In addition, for the first time, wild-type NMRI mice were used for the in vivo mutagenicity assessment applying ecNGS. Nitroso-bisoprolol, the NDSRI of bisoprolol, was negative in standard and modified Ames tests using 10 % induced rat and 30 % uninduced hamster S9, but positive in the Enhanced Ames Test (EAT) in the presence of 30% induced hamster S9, confirming that EAT conditions are more sensitive in detecting the mutagenicity of weakly potent nitrosamines such as NBP. A standard in vitro mammalian cell mutagenicity assay (HPRT) in V79 cells was able to detect the mutagenicity of NDEA, but not that of the more complex low potent NDSRI nitroso-bisoprolol. Our data have shown that nitroso-bisoprolol is a weak in vivo rodent mutagen with a $BMDL_{50}$ of 140 or 96 mg/kg bw/day in bone marrow or liver, respectively. In contrast, a $BMDL_{50}$ of 0.04 mg/kg bw/day was reported for the small potent nitroso-diethylamine (NDEA) (Bercu et al. 2023). Comparison of the mutation fingerprints of NDEA and nitroso-bisoprolol supports a threshold mechanism based on similar DNA repair pathways. Moreover, the mutation spectra of nitroso-bisoprolol and benzo(a)pyrene, a known pro-mutagen, were clearly distinct.

Consistent with regulatory emphasis on mechanistic interpretation, in vivo modeling was further supported by in silico calculations. Specifically, the validated Computer-Aided Discovery and RE-design (CADRE) tool was used to predict the potency of NBP and further differentiate its metabolic activity from the anchor nitrosamine NDEA via quantum mechanics (QM) calculations and CYP-binding predictions. Outcomes of this analysis were consistent with in vivo studies, while offering a deeper understanding of the fundamental biochemistry using a physics-led method. The integrated in vivo–in silico investigation provides a data-based determination of safe limits, suggesting

Table 11 Comparison of mutation fingerprints in NDEA, NPYR, and NBP

Species/tissue	Nitrosamine	C > A	C > G	C > T	T > A	T > C	T > G	Reference
Rat liver	NDEA	NC	NC	Increase	Increase	Increase	Increase	Bercu (2023)
Mouse liver	NDEA	NC	NC	Increase	Increase	Increase	Increase	Zhang (2024)
In vitro (iPSCs)	NPYR	NC	NC	Increase	Increase	NC	NC	Kucab (2019)
Mouse liver	NBP	NC	NC	Increase	Increase	Increase	Increase	Brenneis (2024)
Mouse BM	NBP	NC	NC	Increase	NC	NC	Increase	Brenneis (2024)

NC no change

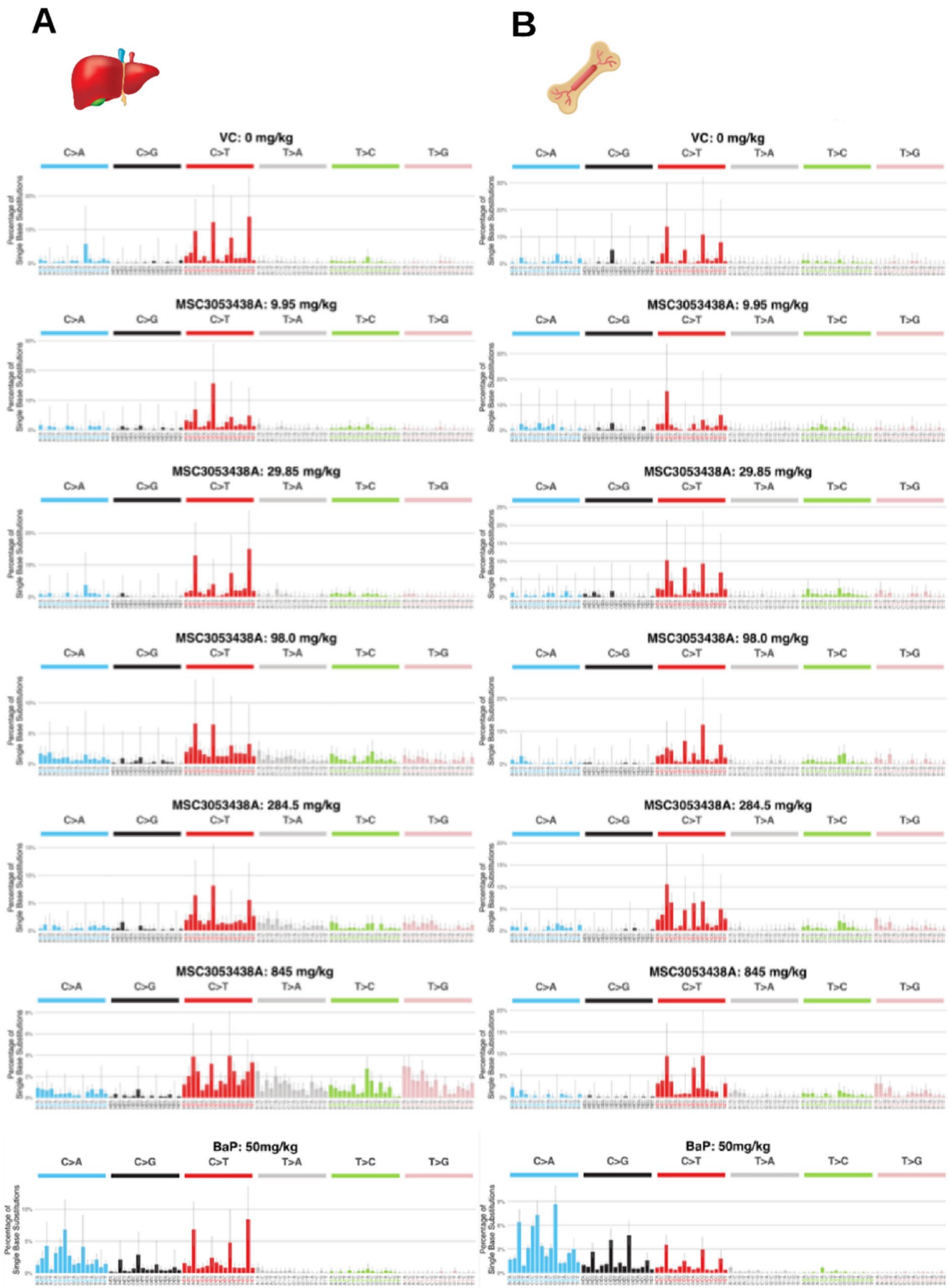
A
B
VC: 0 mg/kg
MSC3053438A: 9.95 mg/kg
MSC3053438A: 29.85 mg/kg
MSC3053438A: 98.0 mg/kg
MSC3053438A: 284.5 mg/kg
MSC3053438A: 845 mg/kg
BaP: 50mg/kg
C>A
C>G
C>T
T>A
T>C
T>G
Percentage of Single Base Substitutions

◂**Fig. 8** Trinucleotide mutation spectra by NBP treatment and BaP group. The proportion (shown as a percentage) of each base substitution type in all trinucleotide contexts (pyrimidine notation) relative to other base substitution types is shown. The frequency of each base substitution type in each context was normalized by the sum of the total single base substitution frequency, so the proportions for each treatment group sum to one. The frequency was derived by dividing the count of each substitution type by the relative abundance (total duplex depth, excluding no-calls) of that context in the regions examined. Error bars represent 95 % binomial proportion Wilson score intervals calculated using the context-specific substitution frequency data. These intervals were also normalized by the sum of the total single base substitution frequencies

that the AI based on structural considerations only might be over-conservative and should not be capped at the TTC. We have used these data to derive substance-specific limits for nitroso-bisoprolol, both in terms of a permissible daily exposure as per ICH Q3C and ICH M7 for substances with a practical threshold in their dose response, and in terms of an acceptable intake based on extrapolation to NDEA. These limits, which are still conservative and providing patient protection, were 400 µg/day (PDE) and 64 µg/day (AI), respectively. Using alternative primary or secondary anchor compounds, such as NMOR, N-Nitroso-Reboxetin, or two further NDSRIs for extrapolation, the AI for NBP will be significantly higher, indicating that using NDEA as anchor yields the most conservative AI. However, development of criteria for appropriate anchor compound selection will be a subject for future evaluations. Our data provide evidence that the currently official SAR/CPCA-based AI for nitroso-bisoprolol of 1.5 µg/day is far too conservative, and that NBP does not belong in the cohort of concern.

The lowest observed effective NBP dose of 29.86 mg/kg bw showing a statistically significant increase in mutation frequency in the bone marrow of mice corresponds to a human equivalent dose (HED) of approximately 2.4 mg/kg bw (or 120 mg/person considering an allometric scaling factor of 0.08 and a standard body weight of 50 kg (FDA 2005)). Of note, the maximum daily dose of bisoprolol is 20 mg/day, and thus, an NBP HED of 120 mg/day is highly hypothetical and cannot be reached under any treatment regimen in patients. Comparing this NBP HED for mutagenic effects to the PDE and AI values of 400 µg/day and 64 µg/day calculated based on the $BDML_{50}$ derived from in vivo mutagenicity data, our proposed limits are 300-fold and 1,875-fold below this NBP HED confirming highly sufficient safety margins. Safety margins above 1000 are generally considered appropriate to ensure patient safety.

Considering the high molecular similarity between the beta-adrenoceptor binding compounds and their respective NDSRIs, it would be justified to use our safe limits for NBP as general class-specific limits for those NDSRIs that bear an isopropyl or tert-butyl group connected to the nitroso group (NDSRIs of Acebutolol, Salbutamol, Atenolol, Betaxolol, Bisoprolol, Celiprolol, Carteolol, Esmolol, Isoproterenol, Levalbuterol, Levobunolol, Metoprolol, Nadolol, Pindolol, Propranolol, Sotalol, and Timolol).

Our analysis was based on ecNGS, which detects mutations across the genome and is superior to the current gold standard TGR in several ways, including speed, costs, and flexibility to name just a few. This lends the methodology to being a natural in vivo follow-up mutagenicity study for nitrosamines, to derive realistic substance-specific safe limits. It allows for the determination of limits across endpoints, i.e., the limit for a potential mutagenic carcinogen can be derived from mutagenicity data, which can be generated much faster and more easily than carcinogenicity data. Considering the magnitude of the NDSRI problem, this approach may be the only option to generate a relevant number of data-based safe limits in the absence of carcinogenicity data. The data we presented here highlight the importance of considering ecNGS methods as alternatives to the TGR. Moreover, the quantitative analysis of in vivo mutagenicity data using BMD modeling to support derivation of regulatory limits, complements the existing approaches and opens space for reconsideration of AIs determined by CPCA by Health Authorities.

Table 12 BMD metrics of covariate vs. non-covariate BMD calculation

	BMDL liver	BMDU liver	BMDL BM	BMDU BM
No covariate	91	255	29	131
NDEA mouse & rat liver as covariates	96	176	140	286
NDEA mouse liver as covariate	96	186	–	–
BaP mouse bone marrow as covariate	–	–	103	283

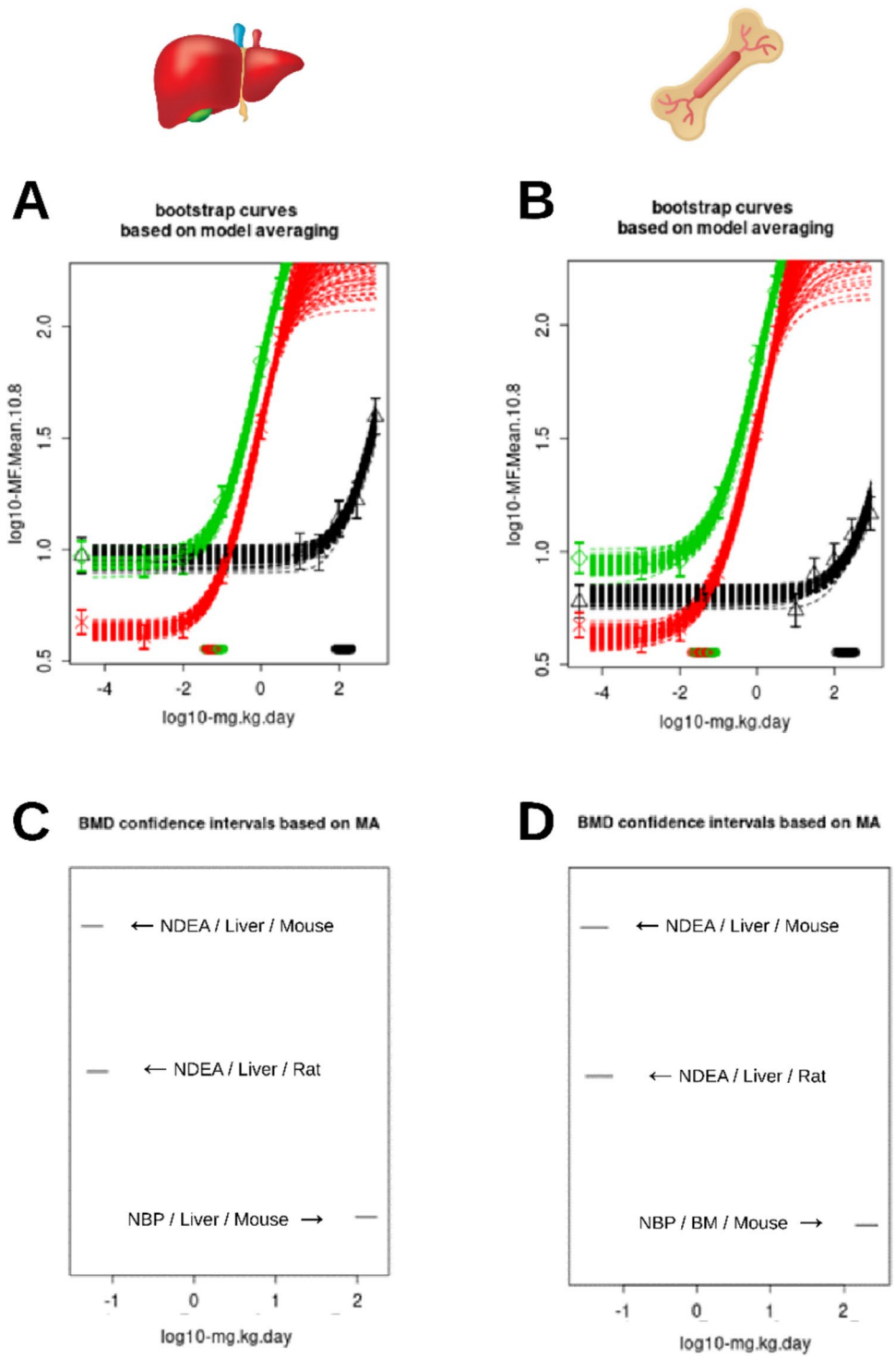

Fig. 9 BMD model averaging analysis of liver (upper left panel) and bone marrow (upper right panel) mutation frequency (MF) and the respective confidence intervals (lower left and right panel). Data for NBP (black) compared to liver NDEA (red) data in mice (Zhang et al. 2024) and rats (green) (Bercu et al. 2023). Note: log10-CED-0.5 is equal to log10-mg/kg/day

Table 13 Permitted daily exposure (PDE) calculation using BMD as PoD

	BMDL Liver	BMDU Liver	BMDL Bone marrow (BM)	BMDU Bone marrow (BM)
BMD_{50} [mg/kg/day]	96	176	140	286
PDE [µg/person/day]	400	733	596	1192

Table 14 Acceptable intakes calculated for NBP based on alternative anchor nitrosamines

Anchor nitrosamine	$BMDL_{50}$ [mg/kg bw/day]	AI anchor [ng/day]	Subjacent anchor	AI NBP [µg/day]	% of AI-based on NDEA	References
NDEA	0.04	26.5	N/A	64	100	Bercu (2023), EMA (2024b)
NMOR	0.024	127	N/A	508	799	Zhang (2025), EMA (2024b)
N-Nitroso-Reboxetine	4.49	24,000	NMOR	513	807	Zhang (2025)

Supplementary Information The online version contains supplementary material available at https://doi.org/10.1007/s00204-025-04103-2.

Acknowledgements The authors express their acknowledgement to A. Gally, S. Hiller, J. Giefer, E. Diehl, A. Wolf, S. Marquardt, and with special thanks to M.-L. Stolz for their experimental support. The authors would like to thank R. Nudelman for critical reading of the manuscript and his valuable comments. Additionally, the authors wish to acknowledge Adelina Voutchkova-Kostal for her significant contributions to the QM modeling and CYP-docking analysis.

Author contributions SSI: conceptualization, investigation, methodology, resources, writing—original draft, and writing—review & editing; JS: writing – original draft, writing – review & editing, and visualization; GJ: investigation, writing—original draft, writing—review & editing; CB: investigation, writing—original draft, writing—review & editing; BG: investigation, writing—original draft, writing—review & editing; JK: investigation, writing—original draft, writing—review & editing, and visualization; JD: investigation, methodology, resources, writing—review & editing, and visualization. All authors reviewed the results and approved the final version of the manuscript.

Funding This research did not receive any specific grant from funding agencies in the public, commercial, or not-for-profit sectors.

Data availability The in vitro and in vivo mutagenicity data presented in this manuscript were also donated to and are available via the Lhasa Vitic complex nitrosamines database (Lhasa Limited 2022). Raw data can be made available upon request.

Declarations

Conflict of interest The authors declare no conflict of interest, financial or otherwise. GJ is a consultant who evaluates the risks posed by pharmaceutical impurities. His clients did not influence the content of this manuscript.

Informed consent The manuscript does not contain clinical studies or patient data.

References

Baum M, Loeppky RN, Thielen S, Eisenbrand G (2008) Genotoxicity of glycidamide in comparison to 3-N-nitroso-oxazolidin-2-one. J Agric Food Chem 56(15):5989–5993. https://doi.org/10.1021/jf703741a

Bercu J, Dirat O, Dobo K et al (2024) N-Nitrosamine drug substance related impurities (NDSRIs)—A proposal for the addition of subcategories to carcinogenic potency categorization approach categories 1 and 2 for NDSRIs with a molecular weight > 200 Da. Regul Toxicol Pharmacol 154:105704. https://doi.org/10.1016/j.yrtph.2024.105704

Bercu J, Trejo-Martin A, Chen C et al (2025) HESI GTTC ring trial: concordance between ames and rodent carcinogenicity outcomes for N-Nitrosamines (NAs) with rat and hamster metabolic conditions. Regulat Toxicol Pharmacol 161:105835. https://doi.org/10.1016/j.yrtph.2025.105835

Bercu JP, Morinello EJ, Sehner C, Shipp BK, Weideman PA (2016) Point of departure (PoD) selection for the derivation of acceptable daily exposures (ADEs) for active pharmaceutical ingredients (APIs). Regul Toxicol Pharmacol 79(Suppl 1):S48-56. https://doi.org/10.1016/j.yrtph.2016.05.028

Bercu JP, Zhang S, Sobol Z, Escobar PA, Van P, Schuler M (2023) Comparison of the transgenic rodent mutation assay, error corrected next generation duplex sequencing, and the alkaline comet assay to detect dose-related mutations following exposure to N-nitrosodiethylamine. Mutat Res Genet Toxicol Environ Mutagen 891:503685. https://doi.org/10.1016/j.mrgentox.2023.503685

Brenneis C (2024) MSC3053438A – 4-week oral mutagenicity study in mice using Duplex-Sequencing. Merck Healthcare KGaA, Darmstadt

Buchwald P (2014) Activity-limiting role of molecular size: size-dependency of maximum activity for P450 inhibition as revealed by qHTS data. Drug Metab Dispos 42(11):1785–1790. https://doi.org/10.1124/dmd.114.059717

Buchwald P, Yamashita F (2014) Bilinear model for the size-dependency of the CYP3A4 inhibitory activity of structurally diverse compounds. Mol Inf 33(1):8–14. https://doi.org/10.1002/minf.201300132

Canada H (2024) Guidance on nitrosamine impurities in medications—Evaluating and managing the risks of N-nitrosamine impurities in human pharmaceutical, biological and radiopharmaceutical products. Adopted 2024-05-31. In: Canada H (ed) H164-327/2024E-1-PDF.

Cross KP, Ponting DJ (2021) Developing structure-activity relationships for N-nitrosamine activity. Comput Toxicol. https://doi.org/10.1016/j.comtox.2021.100186

Dalgaard P R Development Core Team (2010): R: a language and environment for statistical computing. In: 2010

Devaurs D, Antunes DA, Hall-Swan S et al (2019) Using parallelized incremental meta-docking can solve the conformational sampling issue when docking large ligands to proteins. BMC Mol Cell Biol 20(1):42. https://doi.org/10.1186/s12860-019-0218-z

Dodge AE, LeBlanc DPM, Zhou G et al (2023) Duplex sequencing provides detailed characterization of mutation frequencies and spectra in the bone marrow of MutaMouse males exposed to procarbazine hydrochloride. Arch Toxicol 97(8):2245–2259. https://doi.org/10.1007/s00204-023-03527-y

Durairaj P, Fan L, Machalz D, Wolber G, Bureik M (2019) Functional characterization and mechanistic modeling of the human cytochrome P450 enzyme CYP4A22. FEBS Lett 593(16):2214–2225. https://doi.org/10.1002/1873-3468.13489

EMA (2023) Questions and answers for marketing authorisation holders/applicants on the CHMP Opinion for the Article 5(3) of Regulation (EC) No 726/2004 referral on nitrosamine impurities in human medicinal products, Appendix 2: Carcinogenic Potency Categorisation Approach (CPCA) for N-nitrosamines EMA/451665/2023

EMA (2024a) Questions and answers for marketing authorisation holders/applicants on the CHMP Opinion for the Article 5(3) of Regulation (EC) No 726/2004 referral on nitrosamine impurities in human medicinal products, 19 July 2024 EMA/409815/2020 Rev21

EMA (2024b) Questions and answers for marketing authorisation holders/applicants on the CHMP Opinion for the Article 5(3) of Regulation (EC) No 726/2004 referral on nitrosamine impurities in human medicinal products, Appendix 1: Acceptable intakes (AIs) established for N-nitrosamines EMA/307633/2024 /Rev 8

EMA (2024c) Questions and answers for marketing authorisation holders/applicants on the CHMP Opinion for the Article 5(3) of Regulation (EC) No 726/2004 referral on nitrosamine impurities in human medicinal products, Appendix 3: Enhanced Ames Test Conditions for N-nitrosamines EMA/120337/2024

Fahrer J, Christmann M (2023) DNA alkylation damage by nitrosamines and relevant DNA repair pathways. Int J Mol Sci. https://doi.org/10.3390/ijms24054684

Fahrer J, Frisch J, Nagel G et al (2015) DNA repair by MGMT, but not AAG, causes a threshold in alkylation-induced colorectal carcinogenesis. Carcinogenesis 36(10):1235–1244. https://doi.org/10.1093/carcin/bgv114

FDA (2005) Estimating the maximum safe starting dose in initial clinical trials for therapeutics in adult healthy volunteers. Guidance for Industry, July 2005

FDA (2023) Recommended acceptable intake limits for nitrosamine drug substance-related impurities (NDSRIs)—guidance for industry, August 2023

FDA (2024) Control of nitrosamine impurities in human drugs—guidance for industry, Revision 2, September 2024

Guttenplan JB (1990) Mutagenesis by N-nitroso compounds: relationships to DNA adducts, DNA repair, and mutational efficiencies. Mutat Res 233(1–2):177–187. https://doi.org/10.1016/0027-5107(90)90161-v

Hardy A, Benford D, Halldorsson T et al (2017) Guidance on the use of the weight of evidence approach in scientific assessments. EFSA J 15(8):e04971. https://doi.org/10.2903/j.efsa.2017.4971

ICH (2023) ICH harmonized guideline: assessment and control of DNA-reactive (mutagenic) impurities in pharmaceuticals to limit potential carcinogenic risk, M7(R2), Final version, adopted on 3 April 2023

ICH (2024) ICH Harmonized Guideline: Impurities: Guideline for Residual Solvents Q3C(R9), Current Step 4 version, dated 24 January 2024

Jenkins GJ, Doak SH, Johnson GE, Quick E, Waters EM, Parry JM (2005) Do dose response thresholds exist for genotoxic alkylating agents? Mutagenesis 20(6):389–398. https://doi.org/10.1093/mutage/gei054

Johnson GE (2024) S06–02 Consideration of dose-response in the assessment of genotoxic carcinogens. Toxicol Lett 399:S20. https://doi.org/10.1016/j.toxlet.2024.07.061

Johnson GE (2025) N-nitrosobisoprolol (NBP): Benchmark Dose Analysis of an error-corrected Next Generation Sequencing based repeat-dose gene mutation assay in vivo. Version 2; on behalf of Merck Healthcare KGaA

Johnson GE, Dobo K, Gollapudi B et al (2021) Permitted daily exposure limits for noteworthy N-nitrosamines. Environ Mol Mutagen 62(5):293–305. https://doi.org/10.1002/em.22446

Jolly RA, Cornwell PD, Noteboom J, Sayyed FB, Thapa B, Buckley LA (2024) Estimation of acceptable daily intake values based on modeling and in vivo mutagenicity of NDSRIs of fluoxetine, duloxetine and atomoxetine. Regul Toxicol Pharmacol 152:105672. https://doi.org/10.1016/j.yrtph.2024.105672

Jolly RA, Trejo-Martin A, Bercu J, et al. (2025) Ames concordance with the in vivo TGR mutation assay for NDSRIs and relative in vivo TGR potency with exemplar nitrosamines. Regul Toxicol Pharmacol, *in preparation*

Kappel S, Hawkins P, Mendl MT (2017) To group or not to group? Good practice for housing male laboratory mice. Animals 7(12):88

Keane TM, Goodstadt L, Danecek P et al (2011) Mouse genomic variation and its effect on phenotypes and gene regulation. Nature 477(7364):289–294. https://doi.org/10.1038/nature10413

Kostal J (2018) Quantum mechanics approaches in computational toxicology computational toxicology. pp 31–68

Kostal J The HESI QSAR-QM Project: bridging QM methods and the CPCA to enhance hazard assessment of N-nitrosamines In Silico. In: Updates on approaches to acceptable intakes of nitrosamine drug substance related impurities (NDSRIs) and Bioequivalence Assessment for Reformulated Drug Products, Center for Research on Complex Generics, Shady Grove, MD, USA, 2024

Kostal J, Voutchkova-Kostal A (2023) Quantum-mechanical approach to predicting the carcinogenic potency of N-Nitroso impurities in pharmaceuticals. Chem Res Toxicol 36(2):291–304. https://doi.org/10.1021/acs.chemrestox.2c00380

Kostal J, Voutchkova-Kostal A (2025) Tale of three N-nitrosamines and the variables needed to assess their carcinogenicity in silico incorporated into a single workflow. Chem Res Toxicol. https://doi.org/10.1021/acs.chemrestox.4c00482

Kruhlak NL, Schmidt M, Froetschl R et al (2024) Determining recommended acceptable intake limits for N-nitrosamine impurities in pharmaceuticals: development and application of the Carcinogenic Potency Categorization Approach (CPCA). Regul Toxicol Pharmacol 150:105640. https://doi.org/10.1016/j.yrtph.2024.105640

Kucab JE, Zou X, Morganella S et al (2019) A Compendium of mutational signatures of environmental agents. Cell 177(4):821–836. https://doi.org/10.1016/j.cell.2019.03.001

Kuroki T, Drevon C, Montesano R (1977) Microsome-mediated mutagenesis in V79 Chinese hamster cells by various nitrosamines. Cancer Res 37(4):1044–1050

Kuvek T, Marcher C, Berteotti A, Lopez Carrillo V, Schleifer KJ, Oostenbrink C (2024) A computational pipeline observes the flexibility and dynamics of plant cytochrome P450 binding sites. Int J Mol Sci. https://doi.org/10.3390/ijms252111381

Lai Z, Markovets A, Ahdesmaki M et al (2016) VarDict: a novel and versatile variant caller for next-generation sequencing in cancer

research. Nucleic Acids Res 44(11):e108. https://doi.org/10.1093/nar/gkw227
LeBlanc DPM, Meier M, Lo FY et al (2022) Duplex sequencing identifies genomic features that determine susceptibility to benzo(a)pyrene-induced in vivo mutations. BMC Genomics 23(1):542. https://doi.org/10.1186/s12864-022-08752-w
Lhasa Limited (2022) Vitic complex nitrosamines - Understanding the mutagenic potential of structurally-complex (API-like) nitrosamines. https://www.lhasalimited.org/Initiatives/complex-nitrosamines.htm
Lhasa Limited (2024) Lhasa Carcinogenicity Database. https://www.lhasalimited.org/products/lhasa-carcinogenicitydatabase.htm
Lhasa Limited (2025) Vitic Complex Nitrosamines Database
Lynch BJ, Truhlar DG (2004) Small basis sets for calculations of barrier heights, energies of reaction, electron affinities, geometries, and dipole moments. Theoret Chem Acc 111(2):335–344. https://doi.org/10.1007/s00214-003-0518-3
Marchetti F, Cardoso R, Chen CL et al (2023a) Error-corrected next-generation sequencing to advance nonclinical genotoxicity and carcinogenicity testing. Nat Rev Drug Discov 22(3):165–166. https://doi.org/10.1038/d41573-023-00014-y
Marchetti F, Cardoso R, Chen CL et al (2023b) Error-corrected next generation sequencing—promises and challenges for genotoxicity and cancer risk assessment. Mutat Res Rev Mutat Res 792:108466. https://doi.org/10.1016/j.mrrev.2023.108466
Murtagh F, Legendre P (2014) Ward's hierarchical agglomerative clustering method: which algorithms implement ward's criterion?. J Classif 31(3):274–295. https://doi.org/10.1007/s00357-014-9161-z
Nguyen NT, Nguyen TH, Pham TNH et al (2020) Autodock Vina adopts more accurate binding poses but autodock4 forms better binding affinity. J Chem Inf Model 60(1):204–211. https://doi.org/10.1021/acs.jcim.9b00778
Nudelman R, Kocks G, Mouton B et al (2023) The nitrosamine "Saga": lessons learned from five years of scrutiny. Org Process Res Dev 27(10):1719–1735
OECD (2020) OECD Guideline for the Testing of Chemicals, OECD TG 471, Bacterial Reverse Mutation Test, Corrected: 26 June 2020
OECD (2022) OECD Guideline for the Testing of Chemicals, OECD TG 488, Transgenic Rodent Somatic and Germ Cell Gene Mutation Assays. Adopted: 30 June 2022
Ponting DJ, Czich A, Felter SP et al (2024) Control of N-nitrosamine impurities in drug products: progressing the current CPCA framework and supporting the derivation of robust compound specific acceptable intakes. Regul Toxicol Pharmacol 156:105762. https://doi.org/10.1016/j.yrtph.2024.105762
Powley MW, Sobol Z, Johnson GE et al (2024) N-nitrosamine impurity risk assessment in pharmaceuticals: utilizing In vivo mutation relative potency comparison to establish an acceptable intake for NTTP. Regul Toxicol Pharmacol 152:105681. https://doi.org/10.1016/j.yrtph.2024.105681
Roper JM, Griffin TR, Johnson GE, Kostal J, Nudelman R (2025) Using N-nitrosodiethanolamine (NDELA) and N-nitrosopiperidine (NPIP) transgenic rodent gene mutation data and quantum mechanical modeling to derive potency-based acceptable intakes for NDSRIs lacking robust carcinogenicity data. Environ Mol Mutagen *in press*
Salk JJ, Kennedy SR (2020) Next-generation genotoxicology: using modern sequencing technologies to assess somatic mutagenesis and cancer risk. Environ Mol Mutagen 61(1):135–151. https://doi.org/10.1002/em.22342
Schieferdecker S, Vock E (2025) Quantum chemical evaluation and QSAR modeling of N-nitrosamine carcinogenicity. Chem Res Toxicol 38(2):325–339. https://doi.org/10.1021/acs.chemrestox.4c00476
Schlingemann J, Burns MJ, Ponting DJ et al (2023) The landscape of potential small and drug substance related nitrosamines in pharmaceuticals. J Pharm Sci 112(5):1287–1304. https://doi.org/10.1016/j.xphs.2022.11.013
Schuster DM, LeBlanc DPM, Zhou G et al (2024) Dose-related mutagenic and clastogenic effects of benzo[b]fluoranthene in mouse somatic tissues detected by duplex sequencing and the micronucleus assay. Environ Sci Technol 58(49):21450–21463. https://doi.org/10.1021/acs.est.4c07236
Shiizaki K, Kawanishi M, Yagi T (2017) Modulation of benzo[a]pyrene-DNA adduct formation by CYP1 inducer and inhibitor. Genes Environ 39:14. https://doi.org/10.1186/s41021-017-0076-x
Smith-Roe SL, Hobbs CA, Hull V et al (2023a) Adopting duplex sequencing technology for genetic toxicity testing: a proof-of-concept mutagenesis experiment with N-Ethyl-N-Nitrosourea (ENU)-exposed rats bioRxiv. 20230509 edn
Smith-Roe SL, Hobbs CA, Hull V et al (2023b) Adopting duplex sequencing technology for genetic toxicity testing: a proof-of-concept mutagenesis experiment with N-ethyl-N-nitrosourea (ENU)-exposed rats. Mutat Res Genet Toxicol Environ Mutagen 891:503669. https://doi.org/10.1016/j.mrgentox.2023.503669
Su M, Yang Q, Du Y et al (2019) Comparative assessment of scoring functions: the CASF-2016 update. J Chem Inf Model 59(2):895–913. https://doi.org/10.1021/acs.jcim.8b00545
Thielen S, Baum M, Hoffmann M, Loeppky RN, Eisenbrand G (2006) Genotoxicity of glycidamide in comparison to (+/-)-anti-benzo[a]pyrene-7,8-dihydrodiol-9,10-epoxide and alpha-acetoxy-N-nitroso-diethanolamine in human blood and in mammalian V79-cells. Mol Nutr Food Res 50(4–5):430–436. https://doi.org/10.1002/mnfr.200500227
Torrent-Sucarrat M, De Proft F, Ayers PW, Geerlings P (2010) On the applicability of local softness and hardness. Phys Chem Chem Phys 12(5):1072–1080. https://doi.org/10.1039/b919471a
Valentine CC 3rd, Young RR, Fielden MR et al (2020) Direct quantification of in vivo mutagenesis and carcinogenesis using duplex sequencing. Proc Natl Acad Sci U S A 117(52):33414–33425. https://doi.org/10.1073/pnas.2013724117
Voutchkova-Kostal A, Vaccaro S, Kostal J (2022) Computer-aided discovery and redesign for respiratory sensitization: a tiered mechanistic model to deliver robust performance across a diverse chemical space. Chem Res Toxicol 35(11):2097–2106. https://doi.org/10.1021/acs.chemrestox.2c00224
WHO (2023) Web Annex A. World Health Organization Model List of Essential Medicines—23rd List, 2023. In: The selection and use of essential medicines 2023: Executive summary of the report of the 24th WHO Expert Committee on the Selection and Use of Essential Medicines, 24–28 April 2023. Geneva: World Health Organization; 2023 (WHO/MHP/HPS/EML/2023.02). Licence: CC BYNC-SA 3.0 IGO
Wills JW, Johnson GE, Battaion HL, Slob W, White PA (2017) Comparing BMD-derived genotoxic potency estimations across variants of the transgenic rodent gene mutation assay. Environ Mol Mutagen 58(9):632–643. https://doi.org/10.1002/em.22137
Wills JW, Johnson GE, Doak SH, Soeteman-Hernandez LG, Slob W, White PA (2016a) Empirical analysis of BMD metrics in genetic toxicology part I: in vitro analyses to provide robust potency rankings and support MOA determinations. Mutagenesis 31(3):255–263. https://doi.org/10.1093/mutage/gev085
Wills JW, Long AS, Johnson GE et al (2016b) Empirical analysis of BMD metrics in genetic toxicology part II: in vivo potency comparisons to promote reductions in the use of experimental animals for genetic toxicity assessment. Mutagenesis 31(3):265–275. https://doi.org/10.1093/mutage/gew009

Wondrousch D, Böhme A, Thaens D, Ost N, Schüürmann G (2010) Local electrophilicity predicts the toxicity-relevant reactivity of Michael acceptors. J Phys Chem Lett 1(10):1605–1610. https://doi.org/10.1021/jz100247x

Wood DE, Salzberg SL (2014) Kraken: ultrafast metagenomic sequence classification using exact alignments. Genome Biol 15(3):R46. https://doi.org/10.1186/gb-2014-15-3-r46

Zeller A, Duran-Pacheco G, Guerard M (2017) An appraisal of critical effect sizes for the benchmark dose approach to assess dose-response relationships in genetic toxicology. Arch Toxicol 91(12):3799–3807. https://doi.org/10.1007/s00204-017-2037-3

Zeller A, Pfuhler S, Albertini S et al (2018) A critical appraisal of the sensitivity of in vivo genotoxicity assays in detecting human carcinogens. Mutagenesis 33(2):179–193. https://doi.org/10.1093/mutage/gey005

Zhang S, Cheung J, Kostal J, Voutchkova-Kostal A, Schuler M (2025) Re-evaluating acceptable intake: a comparative study of N-Nitrosomorpholine and N-Nitroso reboxetine potency. Environ Mol Mutagen 66(3):80–98. https://doi.org/10.1002/em.70007

Zhang S, Coffing SL, Gunther WC et al (2024) Assessing the genotoxicity of N-nitrosodiethylamine with three in vivo endpoints in male Big Blue(R) transgenic and wild-type C57BL/6N mice Environ Mol Mutagen. 20240716